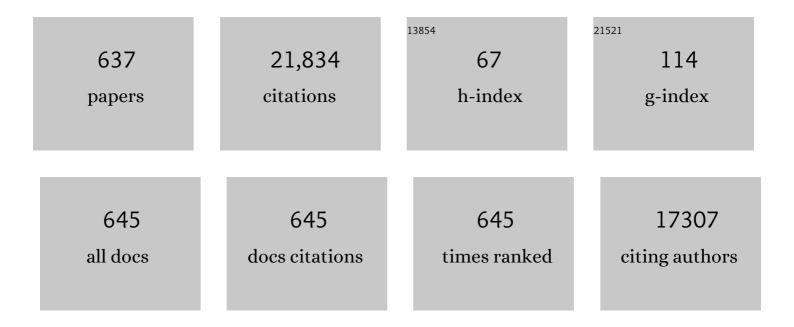
List of Publications by Year in descending order

Source: https://exaly.com/author-pdf/3567149/publications.pdf Version: 2024-02-01



#	Article	IF	CITATIONS
1	Intrinsic and Extrinsic Size Effects in Fineâ€Grained Morphotropicâ€Phaseâ€Boundary Lead Zirconate Titanate Ceramics. Journal of the American Ceramic Society, 1998, 81, 677-688.	1.9	902
2	Relaxor-based ferroelectric single crystals: Growth, domain engineering, characterization and applications. Progress in Materials Science, 2014, 65, 124-210.	16.0	481
3	Elastic, piezoelectric, and dielectric properties of multidomain 0.67Pb(Mg1/3Nb2/3)O3–0.33PbTiO3 single crystals. Journal of Applied Physics, 2001, 90, 3471-3475.	1.1	438
4	Grain size and domain size relations in bulk ceramic ferroelectric materials. Journal of Physics and Chemistry of Solids, 1996, 57, 1499-1505.	1.9	432
5	Back Gated Multilayer InSe Transistors with Enhanced Carrier Mobilities via the Suppression of Carrier Scattering from a Dielectric Interface. Advanced Materials, 2014, 26, 6587-6593.	11.1	410
6	PCR detection and quantitation of predominant anaerobic bacteria in human and animal fecal samples. Applied and Environmental Microbiology, 1996, 62, 1242-1247.	1.4	405
7	The extrinsic nature of nonlinear behavior observed in lead zirconate titanate ferroelectric ceramic. Journal of Applied Physics, 1991, 69, 7219-7224.	1.1	333
8	Theory of tetragonal twin structures in ferroelectric perovskites with a first-order phase transition. Physical Review B, 1991, 44, 5-12.	1.1	298
9	Semiconductor/relaxor 0–3 type composites without thermal depolarization in Bi0.5Na0.5TiO3-based lead-free piezoceramics. Nature Communications, 2015, 6, 6615.	5.8	263
10	An optical temperature sensor based on the upconversion luminescence from Tm3+/Yb3+ codoped oxyfluoride glass ceramic. Sensors and Actuators B: Chemical, 2012, 173, 250-253.	4.0	254
11	Optical temperature sensing through the upconversion luminescence from Ho3+/Yb3+ codoped CaWO4. Sensors and Actuators B: Chemical, 2013, 188, 1096-1100.	4.0	228
12	Losses in ferroelectric materials. Materials Science and Engineering Reports, 2015, 89, 1-48.	14.8	224
13	Ultrahigh photo-responsivity and detectivity in multilayer InSe nanosheets phototransistors with broadband response. Journal of Materials Chemistry C, 2015, 3, 7022-7028.	2.7	203
14	Theoretical model for the morphotropic phase boundary in lead zirconate–lead titanate solid solution. Physical Review B, 1993, 47, 4825-4830.	1.1	186
15	Electric Fatigue in Lead Zirconate Titanate Ceramics. Journal of the American Ceramic Society, 1994, 77, 211-215.	1.9	167
16	Synthesis of two-dimensional β-Ga <sub>2</sub> O <sub>3</sub> nanosheets for high-performance solar blind photodetectors. Journal of Materials Chemistry C, 2014, 2, 3254-3259.	2.7	167
17	Vertical 2D MoO <sub>2</sub> /MoSe <sub>2</sub> Core–Shell Nanosheet Arrays as Highâ€Performance Electrocatalysts for Hydrogen Evolution Reaction. Advanced Functional Materials, 2016, 26, 8537-8544.	7.8	167
18	Piezoelectric ceramic bimorph coupled to thin metal plate as cooling fan for electronic devices. Sensors and Actuators A: Physical, 2000, 79, 8-12.	2.0	166

#	Article	IF	CITATIONS
19	An Insight into the Role of Oxygen Vacancy in Hydrogenated TiO <sub>2</sub> Nanocrystals in the Performance of Dye-Sensitized Solar Cells. ACS Applied Materials & Interfaces, 2015, 7, 3754-3763.	4.0	165
20	Exceptionally High Piezoelectric Coefficient and Low Strain Hysteresis in Grain-Oriented (Ba, Ca)(Ti,) Tj ETQq0 0 Materials & Interfaces, 2017, 9, 29863-29871.	0 rgBT /0 4.0	verlock 10 Tf 5 154
21	Elastic, piezoelectric, and dielectric properties of 0.955Pb(Zn/sub 1/3/Nb/sub 2/3/)O/sub 3/-0.45PbTiO/sub 3/ single crystal with designed multidomains. IEEE Transactions on Ultrasonics, Ferroelectrics, and Frequency Control, 2000, 47, 285-291.	1.7	152
22	Sensitive Electronic-Skin Strain Sensor Array Based on the Patterned Two-Dimensional α-In <sub>2</sub> Se <sub>3</sub> . Chemistry of Materials, 2016, 28, 4278-4283.	3.2	146
23	Short-wavelength upconversion emissions in Ho^3+/Yb^3+ codoped glass ceramic and the optical thermometry behavior. Optics Express, 2012, 20, 18127.	1.7	145
24	Elastic, piezoelectric, and dielectric properties of 0.58Pb(Mg1/3Nb2/3)O3-0.42PbTiO3 single crystal. Journal of Applied Physics, 2004, 96, 549-554.	1.1	141
25	High frequency properties of passive materials for ultrasonic transducers. IEEE Transactions on Ultrasonics, Ferroelectrics, and Frequency Control, 2001, 48, 78-84.	1.7	140
26	Single-domain properties of 0.67Pb(Mg1/3Nb2/3)O3–0.33PbTiO3 single crystals under electric field bias. Applied Physics Letters, 2003, 82, 787-789.	1.5	139
27	Domain-size dependence of piezoelectric properties of ferroelectrics. Physical Review B, 2005, 72, .	1.1	136
28	Excellent optical thermometry based on short-wavelength upconversion emissions in Er^3+/Yb^3+ codoped CaWO_4. Optics Letters, 2012, 37, 4865.	1.7	135
29	Two-Dimensional van der Waals Materials with Aligned In-Plane Polarization and Large Piezoelectric Effect for Self-Powered Piezoelectric Sensors. Nano Letters, 2019, 19, 5410-5416.	4.5	132
30	Highly sensitive optical thermometry through thermally enhanced near infrared emissions from Nd3+/Yb3+ codoped oxyfluoride glass ceramic. Sensors and Actuators B: Chemical, 2013, 178, 520-524.	4.0	127
31	Colorimetric Sensor Based on Selfâ€Assembled Polydiacetylene/Graphene‧tacked Composite Film for Vaporâ€Phase Volatile Organic Compounds. Advanced Functional Materials, 2013, 23, 6044-6050.	7.8	115
32	Highly Stretchable and Conductive Core–Sheath Chemical Vapor Deposition Graphene Fibers and Their Applications in Safe Strain Sensors. Chemistry of Materials, 2015, 27, 6969-6975.	3.2	111
33	Orientation dependence of piezoelectric properties of single domain 0.67Pb(Mn1/3Nb2/3)O3–0.33PbTiO3 crystals. Applied Physics Letters, 2003, 82, 3737-3739.	1.5	106
34	Landau-Ginzburg model of interphase boundaries in improper ferroelastic Perovskites ofD4h18symmetry. Physical Review B, 1990, 41, 4334-4348.	1.1	103
35	The temperature-dependent electrical properties of Bi0.5Na0.5TiO3–BaTiO3–Bi0.5K0.5TiO3 near the morphotropic phase boundary. Acta Materialia, 2012, 60, 469-475.	3.8	100
36	Complete set of material constants of Pb(In1/2Nb1/2)O3–Pb(Mg1/3Nb2/3)O3–PbTiO3 single crystal with morphotropic phase boundary composition. Journal of Applied Physics, 2009, 106, 74112.	1.1	99

#	Article	IF	CITATIONS
37	Domain configurations in domain engineered 0.955Pb(Zn1/3Nb2/3)O3–0.045PbTiO3 single crystals. Journal of Applied Physics, 2000, 87, 7438-7441.	1.1	98
38	Microstructure and ferroelectric properties of MnO2-doped bismuth-layer (Ca,Sr)Bi4Ti4O15 ceramics. Journal of Applied Physics, 2005, 98, 064108.	1.1	98
39	Optical temperature sensing based on the near-infrared emissions from Nd^3+/Yb^3+ codoped CaWO_4. Optics Letters, 2014, 39, 4635.	1.7	98
40	Elastic, dielectric, and piezoelectric constants of Pb(In1/2Nb1/2)O3–Pb(Mg1/3Nb2/3)O3–PbTiO3 single crystal poled along [011]c. Applied Physics Letters, 2010, 97, .	1.5	97
41	Effects of postanneal conditions on the dielectric properties of CaCu3Ti4O12 thin films prepared on Pt/Ti/SiO2/Si substrates. Journal of Applied Physics, 2004, 95, 6483-6485.	1.1	96
42	Large size lead-free (Na,K)(Nb,Ta)O3 piezoelectric single crystal: growth and full tensor properties. CrystEngComm, 2013, 15, 7718.	1.3	94
43	In-Plane Mosaic Potential Growth of Large-Area 2D Layered Semiconductors MoS <sub>2</sub> –MoSe <sub>2</sub> Lateral Heterostructures and Photodetector Application. ACS Applied Materials & Interfaces, 2017, 9, 1684-1691.	4.0	93
44	Title is missing!. Journal of Materials Science Letters, 2002, 21, 1877-1879.	0.5	89
45	Low-Temperature Growth of Large-Area Heteroatom-Doped Graphene Film. Chemistry of Materials, 2014, 26, 2460-2466.	3.2	87
46	Multiâ€Nonvolatile State Resistive Switching Arising from Ferroelectricity and Oxygen Vacancy Migration. Advanced Materials, 2017, 29, 1606165.	11.1	84
47	Influence of dipolar defects on switching behavior in ferroelectrics. Physical Review B, 2000, 63, .	1.1	83
48	Dielectric enhancement and Maxwell-Wagner effects in polycrystalline ferroelectric multilayered thin films. Journal Physics D: Applied Physics, 2001, 34, 2935-2938.	1.3	82
49	Hopping conduction in Mn-doped ZnO. Applied Physics Letters, 2003, 82, 67-69.	1.5	81
50	Characterization of piezoelectric materials with large piezoelectric and electromechanical coupling coefficients. Ultrasonics, 2003, 41, 55-63.	2.1	80
51	Two-/three-dimensional open lanthanide–organic frameworks containing rigid/flexible dicarboxylate ligands: synthesis, crystal structure and photoluminescent properties. CrystEngComm, 2013, 15, 1931.	1.3	79
52	Sonodynamic therapy inhibits angiogenesis and tumor growth in a xenograft mouse model. Cancer Letters, 2013, 335, 93-99.	3.2	77
53	Controlled growth of vertical 3D MoS <sub>2(1â~²x)</sub> Se <sub>2x</sub> nanosheets for an efficient and stable hydrogen evolution reaction. Journal of Materials Chemistry A, 2016, 4, 18060-18066.	5.2	76
54	Domainâ€Related Phase Transitionlike Behavior in Lead Zinc Niobate Relaxor Ferroelectric Single Crystals. Journal of the American Ceramic Society, 1997, 80, 1462-1468.	1.9	75

#	Article	IF	CITATIONS
55	Pinning and depinning mechanism of defect dipoles in PMnN–PZT ceramics. Journal Physics D: Applied Physics, 2005, 38, 1107-1111.	1.3	75
56	Optical Thermometry through Green Upconversion Emissions in Er\$^{3+}\$/Yb\$^{3+}\$-Codoped CaWO\$_{4}\$ Phosphor. Applied Physics Express, 2012, 5, 072201.	1.1	75
57	(K, Na, Li)(Nb, Ta)O <sub>3</sub> :Mn Leadâ€Free Single Crystal with High Piezoelectric Properties. Journal of the American Ceramic Society, 2015, 98, 1829-1835.	1.9	75
58	Giant Negative Electrocaloric Effect in (Pb,La)(Zr,Sn,Ti)O <sub>3</sub> Antiferroelectrics Near Room Temperature. ACS Applied Materials & Interfaces, 2018, 10, 11747-11755.	4.0	75
59	PCR detection ofRuminococcusspp. in human and animal faecal samples. Molecular and Cellular Probes, 1997, 11, 259-265.	0.9	74
60	Sensitive Room Temperature Photoluminescence-Based Sensing of H <sub>2</sub> S with Novel CuO–ZnO Nanorods. ACS Applied Materials & Interfaces, 2016, 8, 16379-16385.	4.0	74
61	Phase diagram and electrostrictive properties of Bi0.5Na0.5TiO3–BaTiO3–K0.5Na0.5NbO3 ceramics. Applied Physics Letters, 2010, 97, .	1.5	73
62	Finite element analysis of the cymbal-type flextensional transducer. IEEE Transactions on Ultrasonics, Ferroelectrics, and Frequency Control, 1998, 45, 1363-1369.	1.7	72
63	Complete set of elastic, dielectric, and piezoelectric coefficents of 0.93Pb(Zn1â^•3Nb2â^•3)O3–0.07PbTiO3 single crystal poled along [011]. Applied Physics Letters, 2006, 89, 242908.	1.5	72
64	Enhanced pyroelectric property in (1â^' <i>x</i> )(Bi <sub>0.5</sub> 0.5)TiO <sub>3</sub> - <i>x</i> Ba(Zr <sub>0.055</sub> Ti <sub> Role of morphotropic phase boundary and ferroelectric-antiferroelectric phase transition. Applied Physics Letters, 2013, 103, 182906.</sub>	0.9451.5	lb>)Q <sub>3&lt; 72</sub>
65	Enhanced Near-Infrared to Visible Upconversion Nanoparticles of Ho <sup>3+</sup> -Yb <sup>3+</sup> -F <sup>–</sup> Tri-Doped TiO <sub>2</sub> and Its Application in Dye-Sensitized Solar Cells with 37% Improvement in Power Conversion Efficiency. Inorganic Chemistry, 2014, 53, 8045-8053.	1.9	71
66	Enhanced NIR-NIR luminescence from CaWO4: Nd3+/Yb3+ phosphors by Li+ codoping for thermometry and optical heating. Journal of Luminescence, 2019, 208, 415-423.	1.5	70
67	Electric field effects on the phase transitions in [001]-oriented(1â^'x)Pb(Mg1/3Nb2/3)O3â^'xPbTiO3single crystals with compositions near the morphotropic phase boundary. Physical Review B, 2003, 68, .	1.1	69
68	Ultrahigh-sensitive optical temperature sensing based on ferroelectric Pr3+-doped (K0.5Na0.5)NbO3. Applied Physics Letters, 2016, 108, .	1.5	69
69	Orientation dependence of piezoelectric properties and mechanical quality factors of 0.27Pb(In1/2Nb1/2)O3-0.46Pb(Mg1/3Nb2/3)O3-0.27PbTiO3:Mn single crystals. Journal of Applied Physics, 2013, 114, .	1.1	68
70	Enhanced electromechanical properties and phase transition temperatures in [001] textured Pb(In1/2Nb1/2)O3-Pb(Mg1/3Nb2/3)O3-PbTiO3 ternary ceramics. Applied Physics Letters, 2015, 107, .	1.5	67
71	CVD growth of large area and uniform graphene on tilted copper foil for high performance flexible transparent conductive film. Journal of Materials Chemistry, 2012, 22, 18283.	6.7	66
72	Complete set of material constants of 0.95(Na0.5Bi0.5)TiO3-0.05BaTiO3 lead-free piezoelectric single crystal and the delineation of extrinsic contributions. Applied Physics Letters, 2013, 103, .	1.5	66

#	Article	IF	CITATIONS
73	Enhanced Piezoelectric Effect Derived from Grain Boundary in MoS <sub>2</sub> Monolayers. Nano Letters, 2020, 20, 201-207.	4.5	66
74	Highâ€Performance [001]câ€Textured PNNâ€PZT Relaxor Ferroelectric Ceramics for Electromechanical Coupling Devices. Advanced Functional Materials, 2020, 30, 2001846.	7.8	66
75	Direct Observation of Ferroelectric Domains in LiTaO3Using Environmental Scanning Electron Microscopy. Physical Review Letters, 1997, 79, 2558-2561.	2.9	65
76	Electroformation of giant unilamellar vesicles using interdigitated ITO electrodes. Journal of Materials Chemistry A, 2013, 1, 7125.	5.2	65
77	Theoretical study on the static performance of piezoelectric ceramicâ€polymer composites with 1â€3 connectivity. Journal of Applied Physics, 1992, 72, 5814-5821.	1.1	62
78	Enhancement of upconversion luminescence of Y2O3:Er3+ nanocrystals by codoping Li+–Zn2+. Journal of Alloys and Compounds, 2011, 509, 409-413.	2.8	62
79	Plane wave propagation in finite $2\hat{a}\in 2$ composites. Journal of Applied Physics, 1995, 78, 4627-4632.	1.1	61
80	Hall effect and dielectric properties of Mn-doped barium titanate. Microelectronic Engineering, 2003, 66, 855-859.	1.1	61
81	Tuning electrochemical catalytic activity of defective 2D terrace MoSe <sub>2</sub> heterogeneous catalyst via cobalt doping. Journal of Materials Chemistry A, 2017, 5, 11357-11363.	5.2	61
82	Ferroelectricity in the ReBa2Cu3O7â~îſ superconductors. Materials Letters, 1988, 6, 317-320.	1.3	59
83	Defect-induced heterogeneous transformations and thermal growth in athermal martensite. Physical Review B, 1990, 41, 11319-11327.	1.1	58
84	Formation mechanism of highly [0 0 1] c textured Pb(In 1/2 Nb 1/2 )O 3 -Pb(Mg 1/3 Nb 2/3 )O 3 -PbTiO 3 relaxor ferroelectric ceramics with giant piezoelectricity. Journal of the European Ceramic Society, 2016, 36, 1973-1981.	2.8	58
85	A complete set of material properties of single domain 0.26Pb(In1/2Nb1/2)O3–0.46Pb(Mg1/3Nb2/3)O3–0.28PbTiO3 single crystals. Applied Physics Letters, 2010, 012907.	96,5	57
86	Optical temperature sensing in Er3+-Yb3+ codoped CaWO4 and the laser induced heating effect on the luminescence intensity saturation. Journal of Alloys and Compounds, 2017, 726, 547-555.	2.8	57
87	Significantly Enhanced Energy-Harvesting Performance and Superior Fatigue-Resistant Behavior in [001] <sub>c</sub> -Textured BaTiO <sub>3</sub> -Based Lead-Free Piezoceramics. ACS Applied Materials & Interfaces, 2018, 10, 31488-31497.	4.0	57
88	Effective macroscopic symmetries and materials properties of multidomain 0.955Pb(Zn1/3Nb2/3)O3-0.045PbTiO3 single crystals. Journal of Applied Physics, 2002, 92, 444-448.	1.1	56
89	Complete set of properties of 0.92Pb(Zn1/3Nb2/3)O3–0.08PbTiO3 single crystal with engineered domains. Materials Letters, 2003, 57, 1305-1308.	1.3	56
90	Solid-State Reaction Synthesis of a InSe/CuInSe <sub>2</sub> Lateral p–n Heterojunction and Application in High Performance Optoelectronic Devices. Chemistry of Materials, 2015, 27, 983-989.	3.2	56

#	Article	IF	CITATIONS
91	Smart materials and structures. Proceedings of the National Academy of Sciences of the United States of America, 1999, 96, 8330-8331.	3.3	55
92	Flux growth and characterization of lead-free piezoelectric single crystal [Bi0.5(Na1â^'xKx)0.5]TiO3. Journal of Crystal Growth, 2005, 281, 364-369.	0.7	55
93	Complete set of elastic, dielectric, and piezoelectric constants of [011]C poled rhombohedral Pb(In0.5Nb0.5)O3-Pb(Mg1/3Nb2/3)O3-PbTiO3:Mn single crystals. Journal of Applied Physics, 2013, 113, 74106.	1.1	55
94	The Predominant Pathway of Apoptosis in THP-1 Macrophage-Derived Foam Cells Induced by 5-Aminolevulinic Acid-Mediated Sonodynamic Therapy is the Mitochondria-Caspase Pathway Despite the Participation of Endoplasmic Reticulum Stress. Cellular Physiology and Biochemistry, 2014, 33, 1789-1801.	1.1	55
95	Inhibition of VDAC1 prevents Ca2+-mediated oxidative stress and apoptosis induced by 5-aminolevulinic acid mediated sonodynamic therapy in THP-1 macrophages. Apoptosis: an International Journal on Programmed Cell Death, 2014, 19, 1712-1726.	2.2	55
96	Enhanced ethanol sensing properties of ultrathin ZnO nanosheets decorated with CuO nanoparticles. Sensors and Actuators B: Chemical, 2018, 255, 3384-3390.	4.0	55
97	Acoustic bandgap formation in a periodic structure with multilayer unit cells. Journal Physics D: Applied Physics, 2000, 33, 1150-1154.	1.3	54
98	Numerical simulations of negative-index refraction in wedge-shaped metamaterials. Physical Review E, 2005, 72, 016607.	0.8	53
99	Detection and photodynamic therapy of inflamed atherosclerotic plaques in the carotid artery of rabbits. Journal of Photochemistry and Photobiology B: Biology, 2011, 102, 26-31.	1.7	53
100	Electromechanical properties and anisotropy of single- and multi-domain 0.72Pb(Mg1/3Nb2/3)O3-0.28PbTiO3 single crystals. Applied Physics Letters, 2011, 99, 162901-1629013.	1.5	53
101	Ultra-large electric field–induced strain in potassium sodium niobate crystals. Science Advances, 2020, 6, eaay5979.	4.7	53
102	The strain limits on switching. Nature Materials, 2005, 4, 727-728.	13.3	52
103	Alumina/epoxy nanocomposite matching layers for high-frequency ultrasound transducer application. IEEE Transactions on Ultrasonics, Ferroelectrics, and Frequency Control, 2009, 56, 213-219.	1.7	52
104	Measurements of face shear properties in relaxor-PbTiO3 single crystals. Journal of Applied Physics, 2011, 110, .	1,1	52
105	Low-intensity Ultrasound Combined with 5-aminolevulinic Acid Administration in the Treatment of Human Tongue Squamous Carcinoma. Cellular Physiology and Biochemistry, 2012, 30, 321-333.	1.1	52
106	1-D helical chain, 2-D layered network and 3-D porous lanthanide–organic frameworks based on multiple coordination sites of benzimidazole-5,6-dicarboxylic acid: synthesis, crystal structure, photoluminescence and thermal stability. CrystEngComm, 2013, 15, 4489.	1.3	52
107	Large field-induced strain, giant strain memory effect, and high thermal stability energy storage in (Pb,La)(Zr,Sn,Ti)O3 antiferroelectric single crystal. Acta Materialia, 2018, 148, 28-37.	3.8	52
108	Grain-Oriented Ferroelectric Ceramics with Single-Crystal-like Piezoelectric Properties and Low Texture Temperature. ACS Applied Materials & Interfaces, 2020, 12, 38415-38424.	4.0	52

#	Article	IF	CITATIONS
109	Multifunctional nanoparticles based on the Nd^3+/Yb^3+ codoped NaYF_4. Optics Letters, 2015, 40, 5678.	1.7	51
110	Noncontact thermometry based on downconversion luminescence from Eu 3+ doped LiNbO 3 single crystal. Sensors and Actuators A: Physical, 2016, 238, 215-219.	2.0	51
111	Ambipolar ferromagnetism by electrostatic doping of a manganite. Nature Communications, 2018, 9, 1897.	5.8	51
112	Acoustic band-gap engineering using finite-size layered structures of multiple periodicity. Applied Physics Letters, 1999, 75, 3713-3715.	1.5	50
113	Hollow Spherical Nanoshell Arrays of 2D Layered Semiconductor for Highâ€Performance Photodetector Device. Advanced Functional Materials, 2018, 28, 1705153.	7.8	50
114	Porous Ultrathin NiSe Nanosheet Networks on Nickel Foam for Highâ€Performance Hybrid Supercapacitors. ChemSusChem, 2020, 13, 260-266.	3.6	50
115	Rapid inhibition of atherosclerotic plaque progression by sonodynamic therapy. Cardiovascular Research, 2019, 115, 190-203.	1.8	49
116	Large electrostrictive effect and high energy storage performance of Pr3+-doped PIN-PMN-PT multifunctional ceramics in the ergodic relaxor phase. Journal of the European Ceramic Society, 2019, 39, 4060-4069.	2.8	49
117	Domain switching and microcracking during poling of lead zirconate titanate ceramics. Ferroelectrics, 1993, 145, 271-281.	0.3	48
118	Luminescence and photosensitivity of gadolinium labeled hematoporphyrin monomethyl ether. Optics Express, 2014, 22, 2414.	1.7	48
119	A high quality lead-free (Li, Ta) modified (K, Na)NbO <sub>3</sub> single crystal and its complete set of elastic, dielectric and piezoelectric coefficients with macroscopic 4mm symmetry. CrystEngComm, 2014, 16, 9828-9833.	1.3	48
120	Coexistence of multiple positive and negative electrocaloric responses in (Pb, La)(Zr, Sn, Ti)O3 single crystal. Applied Physics Letters, 2016, 108, .	1.5	48
121	NaYbF <sub>4</sub> nanoparticles as near infrared light excited inorganic photosensitizers for deep penetration in photodynamic therapy. Nanoscale, 2017, 9, 2706-2710.	2.8	48
122	5-Aminolevulinic Acid-Mediated Sonodynamic Therapy Inhibits RIPK1/RIPK3-Dependent Necroptosis in THP-1-Derived Foam Cells. Scientific Reports, 2016, 6, 21992.	1.6	47
123	Apoptosis of SAS cells induced by sonodynamic therapy using 5-aminolevulinic acid sonosensitizer. Anticancer Research, 2011, 31, 39-45.	0.5	47
124	Quantum cutting mechanism in NaYF_4:Tb^3+, Yb^3+. Optics Letters, 2012, 37, 521.	1.7	46
125	Apoptosis of THP-1 macrophages induced by protoporphyrin IX-mediated sonodynamic therapy. International Journal of Nanomedicine, 2013, 8, 2239. Hysteretic phase transition sequence in <mml:math< td=""><td>3.3</td><td>46</td></mml:math<>	3.3	46

#	Article	IF	CITATIONS
127	5-Aminolevulinic acid-mediated sonodynamic therapy induces anti-tumor effects in malignant melanoma via p53-miR-34a-Sirt1 axis. Journal of Dermatological Science, 2015, 79, 155-162.	1.0	46
128	Generalized continuum theory for ferroelectric thin films. Physical Review B, 2002, 66, .	1.1	45
129	Ultraviolet and violet upconversion luminescence in Ho3+-doped Y2O3 ceramic induced by 532-nm CW laser. Journal of Alloys and Compounds, 2011, 509, 1115-1118.	2.8	45
130	Enhancement of anti-tumor effects of 5-fluorouracil on hepatocellular carcinoma by low-intensity ultrasound. Journal of Experimental and Clinical Cancer Research, 2016, 35, 71.	3.5	45
131	Field-induced phase transitions and enhanced double negative electrocaloric effects in (Pb,La)(Zr,Sn,Ti)O3 antiferroelectric single crystal. Applied Physics Letters, 2018, 112, .	1.5	45
132	Quantum cutting mechanism in Tb3+-Yb3+ co-doped oxyfluoride glass. Journal of Applied Physics, 2011, 110, .	1.1	44
133	Oxygen vacancy induces self-doping effect and metalloid LSPR in non-stoichiometric tungsten suboxide synergistically contributing to the enhanced photoelectrocatalytic performance of WO <sub>3â<sup>^</sup>x</sub> /TiO <sub>2â<sup>^</sup>x</sub> heterojunction. Physical Chemistry Chemical Physics, 2018, 20, 17268-17278.	1.3	44
134	Theoretical study on the static performance of piezoelectric ceramic-polymer composites with 2-2 connectivity. IEEE Transactions on Ultrasonics, Ferroelectrics, and Frequency Control, 1993, 40, 103-109.	1.7	43
135	Analysis of shear modes in a piezoelectric vibrator. Journal of Applied Physics, 1998, 83, 4415-4420.	1.1	43
136	Polarization reversal study using ultrasound. Applied Physics Letters, 2001, 79, 4556-4558.	1.5	43
137	Raman spectroscopy study of ferroelectric modes in [001]-oriented 0.67Pb(Mg1â^•3Nb2â^•3)O3–0.33PbTiO3 single crystals. Applied Physics Letters, 2005, 86, 252903.	1.5	43
138	Fluorescence intensity ratio method for temperature sensing. Optics Letters, 2015, 40, 4544.	1.7	43
139	Antiproliferative and Apoptosis-inducing Effect of exo-Protoporphyrin IX based Sonodynamic Therapy on Human Oral Squamous Cell Carcinoma. Scientific Reports, 2017, 7, 40967.	1.6	43
140	Mechanical-force-induced non-local collective ferroelastic switching in epitaxial lead-titanate thin films. Nature Communications, 2019, 10, 3951.	5.8	43
141	Ultrahigh energy harvesting properties in textured lead-free piezoelectric composites. Journal of Materials Chemistry A, 2019, 7, 3603-3611.	5.2	43
142	Apoptosis of THP-1 Derived Macrophages Induced by Sonodynamic Therapy Using a New Sonosensitizer Hydroxyl Acetylated Curcumin. PLoS ONE, 2014, 9, e93133.	1.1	43
143	Simulation of boundary condition influence in a second-order ferroelectric phase transition. Journal of Applied Physics, 1999, 86, 5739-5746.	1.1	42
144	Complete set of material constants of single domain (K, Na)(Nb, Ta)O3 single crystal and their orientation dependence. Applied Physics Letters, 2014, 105, 212902.	1.5	42

#	Article	IF	CITATIONS
145	A UV light enhanced TiO2/graphene device for oxygen sensing at room temperature. RSC Advances, 2013, 3, 22185.	1.7	41
146	Phase Diagram and Enhanced Piezoelectric Response of Leadâ€Free <scp><scp>BaTiO</scp></scp> <sub>3</sub> – <scp><scp>CaTiO</scp></scp> <sub>3</sub> – <scp>Ba System. Journal of the American Ceramic Society, 2014, 97, 3244-3251.</scp>	Hf <b>Ø</b> <td>&gt;4:1scp&gt;<su< td=""></su<></td>	>4:1scp> <su< td=""></su<>
147	Realization of Subwavelength Asymmetric Acoustic Transmission Based on Low-Frequency Forbidden Transmission. Physical Review Applied, 2016, 5, .	1.5	41
148	Transformed material coefficients for single-domain 0.67Pb(Mg1â^•3Nb2â^•3)O3–0.33PbTiO3 single crystals under differently defined coordinate systems. Applied Physics Letters, 2004, 85, 6380-6382.	1.5	40
149	Superior and coefficients in 0.955Pb(Zn1/3Nb2/3)O3–0.045PbTiO3 and 0.92Pb(Zn1/3Nb2/3)O3–0.08PbTiO3 single crystals poled along [011]. Journal of Physics and Chemistry of Solids, 2004, 65, 1083-1086.	1.9	40
150	Characterization of single domain Pb(In0.5Nb0.5)O3-Pb(Mg1/3Nb2/3)O3-PbTiO3 crystals with monoclinic phase. Journal of Applied Physics, 2011, 110, .	1.1	40
151	Landau expansion parameters for BaTiO3. Journal of Applied Physics, 2013, 114, .	1.1	40
152	Enhance the performance of dye-sensitized solar cells by co-sensitization of 2,6-bis(iminoalkyl)pyridine and N719. RSC Advances, 2013, 3, 25908.	1.7	40
153	Characterization of the performance of 1–3 type piezocomposites for lowâ€frequency applications. Journal of Applied Physics, 1993, 73, 1403-1410.	1.1	39
154	Effective material properties in twinned ferroelectric crystals. Journal of Applied Physics, 1999, 86, 1073-1081.	1.1	39
155	Dielectric enhancement of sol–gel derived BaTiO3/SrTiO3 multilayered thin films. Thin Solid Films, 2002, 406, 113-117.	0.8	39
156	Luminescent La2O2S:Eu3+ nanoparticles as non-contact optical temperature sensor in physiological temperature range. Materials Letters, 2015, 143, 98-100.	1.3	39
157	Electromechanical properties of Mn-doped Pb(In1/2Nb1/2)O3-Pb(Mg1/3Nb2/3)O3-PbTiO3 piezoelectric ceramics. Ceramics International, 2016, 42, 15332-15337.	2.3	39
158	Metallic tungsten carbide nanoparticles as a near-infrared-driven photocatalyst. Journal of Materials Chemistry A, 2019, 7, 18538-18546.	5.2	39
159	Phase transition and dielectric properties of nanograin BaTiO3 ceramic under high pressure. Applied Physics Letters, 2008, 92, .	1.5	38
160	Potentiation of Scutellarin on Human Tongue Carcinoma Xenograft by Low-Intensity Ultrasound. PLoS ONE, 2013, 8, e59473.	1.1	38
161	Effects of 5-aminolevulinic acid-mediated sonodynamic therapy on macrophages. International Journal of Nanomedicine, 2013, 8, 669.	3.3	38
162	Effects of Mn doping on multiferroic and magnetocapacitive properties of 0.33Ba0.70Ca0.30TiO3–0.67BiFeO3 diphasic ceramics. Journal of Alloys and Compounds, 2014, 590, 346-354.	2.8	38

#	Article	IF	CITATIONS
163	Optical thermometry based on the red upconversion fluorescence of Er^3+ in CaWO_4:Yb^3+/Er^3+ polycrystalline powder. Optics Letters, 2016, 41, 1458.	1.7	38
164	Inhibitory effect of aloe emodin mediated photodynamic therapy on human oral mucosa carcinoma in vitro and in vivo. Biomedicine and Pharmacotherapy, 2018, 97, 697-707.	2.5	38
165	Sinoporphyrin sodium based sonodynamic therapy induces anti-tumor effects in hepatocellular carcinoma and activates p53/caspase 3 axis. International Journal of Biochemistry and Cell Biology, 2019, 113, 104-114.	1.2	38
166	<title>Characterization of piezoelectric materials using ultrasonic and resonant techniques</title> . , 1998, 3341, 154.		37
167	Oxygen-related dielectric relaxation and leakage characteristics of Pt/(Ba,Sr)TiO3/Pt thin-film capacitors. Applied Physics Letters, 2002, 80, 2538-2540.	1.5	37
168	Interweaving domain configurations in [001]-poled rhombohedral phase 0.68Pb(Mg1/3Nb2/3)O3–0.32PbTiO3 single crystals. Applied Physics Letters, 2003, 83, 2040-2042.	1.5	37
169	Optimization of piezoelectric properties for [001]c poled 0.94Pb(Zn1/3Nb2/3)O3–0.06PbTiO3 single crystals. Applied Physics Letters, 2010, 96, 92902.	1.5	37
170	Sonodynamic Effect of an Anti-Inflammatory Agent – Emodin onÂMacrophages. Ultrasound in Medicine and Biology, 2011, 37, 1478-1485.	0.7	37
171	The Sonodynamic Effect of Curcumin on THP-1 Cell-Derived Macrophages. BioMed Research International, 2013, 2013, 1-9.	0.9	37
172	Electric field induced metastable ferroelectric phase and its behavior in (Pb, La)(Zr, Sn, Ti)O3 antiferroelectric single crystal near morphotropic phase boundary. Applied Physics Letters, 2014, 104, .	1.5	37
173	Influence of gas inertia and edge effect on squeeze film in near field acoustic levitation. Applied Physics Letters, 2010, 96, .	1.5	36
174	Elastic, dielectric and piezoelectric characterization of single domain PIN-PMN-PT: Mn crystals. Journal of Applied Physics, 2012, 112, 124113.	1.1	36
175	Complete matrix properties of [001]c and [011]c poled 0.33Pb(In1/2Nb1/2)O3–0.38Pb(Mg1/3Nb2/3)O3–0.29PbTiO3 single crystals. Journal of Alloys and Compounds, 2013, 553, 267-269.	2.8	36
176	Aspect ratio dependence of electromechanical coupling coefficient of piezoelectric resonators. Applied Physics Letters, 2005, 87, 132901.	1.5	35
177	Hematoporphyrin monomethyl ether-mediated photodynamic effects on THP-1 cell-derived macrophages. Journal of Photochemistry and Photobiology B: Biology, 2010, 101, 9-15.	1.7	35
178	Effects of sintering temperature and poling conditions on the electrical properties of Ba0.70Ca0.30TiO3 diphasic piezoelectric ceramics. Ceramics International, 2013, 39, 2967-2973.	2.3	35
179	Sonodynamic effects of hematoporphyrin monomethyl ether on <i>Staphylococcus aureus in vitro</i> . FEMS Microbiology Letters, 2014, 361, 174-180.	0.7	35
180	Growth and properties of Li, Ta modified (K,Na)NbO <sub>3</sub> leadâ€free piezoelectric single crystals. Physica Status Solidi - Rapid Research Letters, 2014, 8, 86-90.	1.2	35

#	Article	IF	CITATIONS
181	Tunable passband in one-dimensional phononic crystal containing a piezoelectric 0.62Pb(Mg1/3Nb2/3)O3–0.38PbTiO3 single crystal defect layer. Physica E: Low-Dimensional Systems and Nanostructures, 2014, 60, 37-41.	1.3	35
182	Temperature and electric-field induced phase transitions, and full tensor properties of[011]C-poled domain-engineered tetragonal0.63Pb(Mg1/3Nb2/3)â^'0.37PbTiO3single crystals. Physical Review B, 2016, 93, .	1.1	35
183	794 nm excited core–shell upconversion nanoparticles for optical temperature sensing. RSC Advances, 2016, 6, 11795-11801.	1.7	35
184	The Ratio of Rhombohedral and Tetragonal Phases on the Morphotropic Phase Boundary in Lead Zirconate Titanate. Japanese Journal of Applied Physics, 1992, 31, 1399-1402.	0.8	34
185	Coercive field of 0.955Pb(Zn1/3Nb2/3)O3–0.045PbTiO3 single crystal and its frequency dependence. Applied Physics Letters, 2002, 80, 1043-1045.	1.5	34
186	Elastic, Dielectric and Piezoelctric Coefficients of Domain Engineered 0.70Pb(Mg1/3Nb2/3)O3-0.30PbTiO3 Single Crystal. AIP Conference Proceedings, 2002, , .	0.3	34
187	Evaluation of a web-based intervention for improving HIV/AIDS knowledge in rural Yunnan, China. Aids, 2007, 21, S137-S142.	1.0	34
188	Soft-lithographic processed soluble micropatterns of reduced graphene oxide for wafer-scale thin film transistors and gas sensors. Journal of Materials Chemistry, 2012, 22, 714-718.	6.7	34
189	Characterization of full set material constants of piezoelectric materials based on ultrasonic method and inverse impedance spectroscopy using only one sample. Journal of Applied Physics, 2013, 114, 104505.	1.1	34
190	Phase transition behavior and high piezoelectric properties in lead-free BaTiO3–CaTiO3–BaHfO3 ceramics. Journal of Materials Science, 2014, 49, 62-69.	1.7	34
191	Rapid stabilisation of atherosclerotic plaque with 5-aminolevulinic acid-mediated sonodynamic therapy. Thrombosis and Haemostasis, 2015, 114, 793-803.	1.8	34
192	Patterned Growth of Pâ€Type MoS <sub>2</sub> Atomic Layers Using Sol–Gel as Precursor. Advanced Functional Materials, 2016, 26, 6371-6379.	7.8	34
193	Water-soluble gadolinium porphyrin as a multifunctional theranostic agent: Phosphorescence-based oxygen sensing and photosensitivity. Dyes and Pigments, 2017, 142, 465-471.	2.0	34
194	<i>In-situ</i> observation of the domain configurations during the phase transitions in barium titanate. The Philosophical Magazine: Physics of Condensed Matter B, Statistical Mechanics, Electronic, Optical and Magnetic Properties, 1996, 74, 25-36.	0.6	33
195	Finite element study on 1-D array transducer design. IEEE Transactions on Ultrasonics, Ferroelectrics, and Frequency Control, 2000, 47, 949-955.	1.7	33
196	Anisotropy in domain engineered 0.92Pb(Zn/sub 1/3/Nb/sub 2/3/)O/sub 3/-0.08PbTiO/sub 3/ single crystal and analysis of its property fluctuations. IEEE Transactions on Ultrasonics, Ferroelectrics, and Frequency Control, 2002, 49, 1622-1627.	1.7	33
197	Influence of Yb3+ concentration on upconversion luminescence of Ho3+. Optics Communications, 2011, 284, 1053-1056.	1.0	33
198	Face shear piezoelectric properties of relaxor-PbTiO3 single crystals. Applied Physics Letters, 2011, 98, 182903.	1.5	33

#	Article	IF	CITATIONS
199	Morphology-controlled synthesis of Ag nanoparticle decorated poly(o-phenylenediamine) using microfluidics and its application for hydrogen peroxide detection. Chemical Engineering Journal, 2015, 268, 102-108.	6.6	33
200	5-Aminolevulinic Acid-Based Sonodynamic Therapy Induces the Apoptosis of Osteosarcoma in Mice. PLoS ONE, 2015, 10, e0132074.	1.1	33
201	Elastic constants ofKMnF3as functions of temperature and pressure. Physical Review B, 1988, 38, 7947-7958.	1.1	32
202	Quasi-one-dimensional solutions for domain walls and their constraints in improper ferroelastics. Physical Review B, 1990, 42, 6396-6401.	1.1	32
203	Characterization of lead zirconate titanate piezoceramic using high frequency ultrasonic spectroscopy. Journal of Applied Physics, 1999, 85, 8083-8091.	1.1	32
204	Size dependence of domain patterns in a constrained ferroelectric system. Journal of Applied Physics, 2001, 89, 8105-8109.	1.1	32
205	Electromechanical coupling coefficient of an ultrasonic array element. Journal of Applied Physics, 2006, 99, 074102.	1.1	32
206	Influence of manganese doping to the full tensor properties of 0.24Pb(In1/2Nb1/2)O3-0.47Pb(Mg1/3Nb2/3)O3-0.29PbTiO3 single crystals. Journal of Applied Physics, 2013, 113, 74108.	1.1	32
207	Upconversion nanoparticle-mediated photodynamic therapy induces THP-1 macrophage apoptosis via ROS bursts and activation of the mitochondrial caspase pathway. International Journal of Nanomedicine, 2015, 10, 3719.	3.3	32
208	Temperature dependence of self-consistent full matrix material constants of lead zirconate titanate ceramics. Applied Physics Letters, 2015, 106, 052902.	1.5	32
209	A precise Boltzmann distribution law for the fluorescence intensity ratio of two thermally coupled levels. Applied Physics Letters, 2016, 108, .	1.5	32
210	Origin of Improvement in Mechanical Quality Factor in Acceptor-Doped Relaxor-Based Ferroelectric Single Crystals. Physical Review Applied, 2018, 9, .	1.5	32
211	A simple modification of near-infrared photon-to-electron response with fluorescence resonance energy transfer for dye-sensitized solar cells. Journal of Power Sources, 2014, 264, 254-261.	4.0	31
212	Quantitative monitoring of the level of singlet oxygen using luminescence spectra of phosphorescent photosensitizer. Optics Express, 2015, 23, 22991.	1.7	31
213	Temperature dependence of electric-field-induced domain switching in 0.7Pb(Mg1/3Nb2/3)O3–0.3PbTiO3 single crystal. Journal of Alloys and Compounds, 2012, 527, 101-105.	2.8	30
214	Enhanced Multiferroic and Magnetocapacitive Properties of (1Ââ^'Â <i>x</i> ) <scp><scp>Ba</scp></scp> <sub>0.7</sub> <scp><scp>Ca</scp></scp> <sub>0.3</sub> <scp> Ceramics. Journal of the American Ceramic Society, 2014, 97, 816-825.</scp>	<sc<b>p9TiO∢</sc<b>	<
215	5-Aminolevulinic Acid–mediated Sonodynamic Therapy Reverses Macrophage and Dendritic Cell Passivity in Murine Melanoma Xenografts. Ultrasound in Medicine and Biology, 2014, 40, 2125-2133.	0.7	30
216	High piezoelectricity of Eu <sup>3+</sup> -doped Pb(Mg <sub>1/3</sub> Nb <sub>2/3</sub> )O <sub>3</sub> –0.25PbTiO <sub>3</sub> transparent ceramics. Journal of Materials Chemistry C, 2021, 9, 2426-2436.	2.7	30

#	Article	IF	CITATIONS
217	High-performance Pb(Ni1/3Nb2/3)O3-PbZrO3-PbTiO3 ceramics with the triple point composition. Journal of the European Ceramic Society, 2021, 41, 6983-6990.	2.8	30
218	Complete set of material properties of single domain 0.24Pb(In1/2Nb1/2)O3-0.49Pb(Mg1/3Nb2/3)O3-0.27PbTiO3 single crystal and the orientation effects. Applied Physics Letters, 2011, 99, 32901-329013.	1.5	29
219	Improved thermal stability of [001]c poled 0.24Pb(In1/2Nb1/2)O3–0.47Pb(Mg1/3Nb2/3)O3–0.29PbTiO3 sing crystal with manganese doping. Journal of Alloys and Compounds, 2014, 601, 154-157.	gle 2.8	29
220	Photophysical properties, singlet oxygen generation efficiency and cytotoxic effects of aloe emodin as a blue light photosensitizer for photodynamic therapy in dermatological treatment. Photochemical and Photobiological Sciences, 2017, 16, 1088-1094.	1.6	29
221	Temperature and frequency dependence of the coercive field of 0.71PbMb1/3Nb2/3O3–0.29PbTiO3 relaxor-based ferroelectric single crystal. Applied Physics Letters, 2017, 111, .	1.5	29
222	Improved green upconversion emissions from CaWO4: Er3+-Yb3+ by Cr3+ codoping for optical thermometry. Journal of Luminescence, 2019, 215, 116617.	1.5	29
223	Electromechanical properties of fine-grain, 0.7 Pb(Mg/sub 1/3/Nb/sub 2/3/)O/sub 3/-0.3PbTiO/sub 3/ ceramics. IEEE Transactions on Ultrasonics, Ferroelectrics, and Frequency Control, 2004, 51, 908-912.	1.7	28
224	N,N′-Bis((6-methoxylpyridin-2-yl)methylene)-p-phenylenediimine based d <sup>10</sup> transition metal complexes and their utilization in co-sensitized solar cells. Dalton Transactions, 2014, 43, 11361-11370.	1.6	28
225	Temperature dependence of dielectric and electromechanical properties of (K,Na)(Nb,Ta)O3 single crystal and corresponding domain structure evolution. Journal of Applied Physics, 2014, 116, 044105.	1.1	28
226	Electric field induced phase transition and domain structure evolution in (Pb, La)(Zr, Sn, Ti)O3 single crystal. Applied Physics Letters, 2015, 107, .	1.5	28
227	Electric field and frequency dependent scaling behavior of dynamic hysteresis in relaxor-based ferroelectric 0.71Pb(Mg1/3Nb2/3)O3–0.29PbTiO3 single crystal. Journal of Alloys and Compounds, 2019, 775, 435-440.	2.8	28
228	Piezoelectric performance of piezoceramic-polymer composites with 2-2 connectivity-a combined theoretical and experimental study. IEEE Transactions on Ultrasonics, Ferroelectrics, and Frequency Control, 1994, 41, 556-564.	1.7	27
229	Ferroelectric properties of neodymium-doped Bi4Ti3O12 thin films crystallized in different environments. Thin Solid Films, 2005, 471, 35-39.	0.8	27
230	Optical interband transitions in relaxor-based ferroelectric 0.93Pb(Zn1/3Nb2/3)O3–0.07PbTiO3 single crystal. Journal of Applied Physics, 2010, 107, 113532.	1.1	27
231	Conductive Upconversion Er,Yb-FTO Nanoparticle Coating To Replace Pt as a Low-Cost and High-Performance Counter Electrode for Dye-Sensitized Solar Cells. ACS Applied Materials & Interfaces, 2014, 6, 8223-8229.	4.0	27
232	Temperature induced phase transformations and negative electrocaloric effect in (Pb,La)(Zr,Sn,Ti)O3 antiferroelectric single crystal. Journal of Applied Physics, 2017, 122, .	1.1	27
233	Intrinsic Dipole Coupling in 2D van der Waals Ferroelectrics for Gateâ€Controlled Switchable Rectifier. Advanced Electronic Materials, 2020, 6, 1900975.	2.6	27
234	Nonlinear properties of lead zirconate–titanate piezoceramics. Journal of Applied Physics, 2000, 88, 6684-6689.	1.1	26

#	Article	IF	CITATIONS
235	Effect of surface induced nucleation of ferroelastic domains on polarization switching in constrained ferroelectrics. Journal of Applied Physics, 2003, 93, 537-544.	1.1	26
236	Permissible symmetries of multi-domain configurations in perovskite ferroelectric crystals. Journal of Applied Physics, 2003, 94, 3436-3445.	1.1	26
237	Origin of piezoelectric response under a biased scanning probe microscopy tip across a 180 <mml:math display="inline" xmlns:mml="http://www.w3.org/1998/Math/MathML"><mml:msup><mml:mrow /&gt;<mml:mo>â~</mml:mo></mml:mrow </mml:msup></mml:math> ferroelectric domain wall. Physical Review B, 2012, 86,	1.1	26
238	A face-shear mode single crystal ultrasonic motor. Applied Physics Letters, 2013, 102, .	1.5	26
239	Based on Cu(II) silicotungstate modified photoanode with long electron lifetime and enhanced performance in dye sensitized solar cells. Journal of Power Sources, 2015, 278, 527-533.	4.0	26
240	Field induced phase transitions and energy harvesting performance of (Pb,La)(Zr,Sn,Ti)O3 single crystal. Journal of Applied Physics, 2017, 121, .	1.1	26
241	Hematoporphyrin monomethyl ether mediated sonodynamic antimicrobial chemotherapy on porphyromonas gingivalis in vitro. Microbial Pathogenesis, 2020, 144, 104192.	1.3	26
242	Directional Acoustic Wave Manipulation by a Porpoise via Multiphase Forehead Structure. Physical Review Applied, 2017, 8, .	1.5	26
243	Piezoelectric response of engineered domains in ferroelectrics. Applied Physics Letters, 2004, 84, 3450-3452.	1.5	25
244	Modeling and experimental study on near-field acoustic levitation by flexural mode. IEEE Transactions on Ultrasonics, Ferroelectrics, and Frequency Control, 2009, 56, 2679-2685.	1.7	25
245	From two-dimensional trapezoid-like layer to three-dimensional porous indium-4,4′-biphenyldicarboxylate MOFs. CrystEngComm, 2012, 14, 193-199.	1.3	25
246	Photoluminescence and Temperature Dependent Electrical Properties of Erâ€Doped 0.94 <scp><scp>Bi</scp><sub>0.5</sub><scp><scp>Na</scp>0.5<scp>TiOCeramics. Journal of the American Ceramic Society, 2014, 97, 3877-3882.</scp></scp></scp>	cp1.dscb;	> <s<b>¤b&gt;3</s<b>
247	Luminescence ratiometric oxygen sensor based on gadolinium labeled porphyrin and filter paper. Sensors and Actuators B: Chemical, 2015, 215, 405-411.	4.0	25
248	The efficacy and mechanism of apoptosis induction by hypericin-mediated sonodynamic therapy in THP-1 macrophages. International Journal of Nanomedicine, 2015, 10, 821.	3.3	25
249	Mn doping effects on electric properties of 0.93(Bi <sub>0.5</sub> Na <sub>0.5</sub> )TiO <sub>3</sub> â€0.07Ba(Ti <sub>0.945</sub> Zr <sub>0.055ceramics. Journal of the American Ceramic Society, 2018, 101, 2996-3004.</sub>	ວ>) <b>Ω</b> Զsub	>3 <b>⁄/s</b> ub>
250	Glass-bonded composites containing superconducting YBa2Cu3O9â^'y for levitation and magnetic shielding applications. Materials Research Bulletin, 1988, 23, 623-630.	2.7	24
251	Silicon oxide colloidalâ^•polymer nanocomposite films. Applied Physics Letters, 2004, 85, 5998-6000.	1.5	24
252	Femtosecond pulsed laser induced synthesis of ultrafine Y2O3: Pr, Yb nanoparticles with improved upconversion efficiency. Chemical Physics Letters, 2010, 496, 316-320.	1.2	24

#	Article	IF	CITATIONS
253	Low-temperature sol–gel-derived nanosilver-embedded silane coating as biofilm inhibitor. Nanotechnology, 2011, 22, 155602.	1.3	24
254	Modeling characterization and optimization design for PZT transducer used in Near Field Acoustic Levitation. Sensors and Actuators A: Physical, 2011, 171, 260-265.	2.0	24
255	Morphotropic phase boundary and electric properties in (1â^ <i>x</i> )Bi0.5Na0.5TiO3- <i>x</i> BiCoO3 lead-free piezoelectric ceramics. Journal of Applied Physics, 2012, 111, .	1.1	24
256	Phase transitions and domain evolution in (Pb, La)(Zr, Sn, Ti)O3 single crystal. Applied Physics Letters, 2012, 101, .	1.5	24
257	Three new metal–organic frameworks based on 2-propyl-1H-imidazole-4,5-dicarboxylate: Synthesis, crystal structure and luminescent properties. Polyhedron, 2012, 33, 90-96.	1.0	24
258	Incident fluence dependent morphologies, photoluminescence and optical oxygen sensing properties of ZnO nanorods grown by pulsed laser deposition. Journal of Materials Chemistry C, 2015, 3, 2557-2562.	2.7	24
259	White-light-emitting properties of SrTiO <sub>3</sub> :Pr <sup>3+</sup> nanoparticles. RSC Advances, 2015, 5, 27491-27495.	1.7	24
260	Oxygen sensing properties of gadolinium labeled hematoporphyrin monomethyl ether based on filter paper. Sensors and Actuators B: Chemical, 2015, 206, 351-356.	4.0	24
261	Phase coexistence and domain configuration in Pb(Mg1/3Nb2/3)O3-0.34PbTiO3 single crystal revealed by synchrotron-based X-ray diffractive three-dimensional reciprocal space mapping and piezoresponse force microscopy. Applied Physics Letters, 2016, 108, .	1.5	24
262	Temperature and concentration effects on upconversion photoluminescence properties of Ho3+ and Yb3+ codoped 0.67Pb(Mg1/3Nb2/3)O3–0.33PbTiO3 multifunctional ceramics. Ceramics International, 2016, 42, 11309-11313.	2.3	24
263			

#	Article	IF	CITATIONS
271	Effect of A-site La <sup>3+</sup> modified on dielectric and energy storage properties in lead zironate stannate titanate ceramics. Materials Research Express, 2014, 1, 045501.	0.8	22
272	A biomimetic projector with high subwavelength directivity based on dolphin biosonar. Applied Physics Letters, 2014, 105, .	1.5	22
273	Phase transitional behavior and electrical properties of Pb(In1/2Nb1/2)O3–Pb(Mg1/3Nb2/3)O3–PbTiO3 ternary ceramics. Journal of Materials Science: Materials in Electronics, 2015, 26, 1874-1880.	1.1	22
274	Comparison study on the influence of the central metal ions in palladium( <scp>ii</scp> )- and gadolinium( <scp>iii</scp> )-porphyrins for phosphorescence-based oxygen sensing. Journal of Materials Chemistry C, 2016, 4, 9581-9587.	2.7	22
275	Pr <sup>3+</sup> -Doped (K <sub>0.5</sub> Na <sub>0.5</sub> )NbO <sub>3</sub> as a high response optical oxygen sensing agent. Journal of Materials Chemistry C, 2016, 4, 11508-11513.	2.7	22
276	Densification behavior and electrical properties of CuO-doped Pb(In 1/2 Nb 1/2 )O 3 –Pb(Mg 1/3 Nb 2/3 )O 3 –PbTiO 3 ternary ceramics. Ceramics International, 2016, 42, 7223-7229.	2.3	22
277	Ratiometric dissolved oxygen sensitive indicator based on lutetium labeled hematoporphyrin monomethyl ether with balanced phosphorescence and fluorescence dual emission. Sensors and Actuators B: Chemical, 2016, 231, 539-546.	4.0	22
278	Relaxation behavior in 0.24Pb(In1/2Nb1/2)O3–0.49Pb(Mg1/3Nb2/3)O3–0.27PbTiO3 ferroelectric single crystal. Ceramics International, 2016, 42, 4893-4898.	2.3	22
279	Frequency dependence of the coercive field of 0.71Pb(Mg1/3Nb2/3)O3-0.29PbTiO3 single crystal from 0.01 Hz to 5 MHz. Applied Physics Letters, 2017, 110, 202904.	1.5	22
280	Effect of Mn-doping on dielectric relaxation behavior of Pb(In1/2Nb1/2)O3-Pb(Mg1/3Nb2/3)O3-PbTiO3 ferroelectric ceramics. Ceramics International, 2017, 43, 16819-16826.	2.3	22
281	Origin of large electrostrain in Sn4+ doped Ba(Zr0.2Ti0.8)O3-x(Ba0.7Ca0.3)TiO3 ceramics. Acta Materialia, 2018, 157, 155-164.	3.8	22
282	Plasmonic Enhanced Reactive Oxygen Species Activation on Lowâ€Workâ€Function Tungsten Nitride for Direct Nearâ€Infrared Driven Photocatalysis. Small, 2020, 16, e2004557.	5.2	22
283	Large, thermally stabilized and fatigue-resistant piezoelectric strain response in textured relaxor-PbTiO <sub>3</sub> ferroelectric ceramics. Journal of Materials Chemistry C, 2021, 9, 2008-2015.	2.7	22
284	A transmission electron microscopy investigation of the R3m → R3c phase transition in Pb(Zr,Ti)O3 ceramics. Solid State Communications, 1993, 85, 193-195.	0.9	21
285	Dielectric relaxation of shallow donor in polycrystalline Mn-doped ZnO. Journal of Applied Physics, 2003, 93, 4097-4103.	1.1	21
286	Constructing Landau-Ginzburg-Devonshire Type Models for Ferroelectric Systems Based on Symmetry. Ferroelectrics, 2008, 375, 28-39.	0.3	21
287	Accurate thermometry based on the red and green fluorescence intensity ratio in NaYF_4: Yb, Er nanocrystals for bioapplication. Optics Letters, 2016, 41, 4664.	1.7	21
288	Anti-Stokes excited Er3+/Yb3+ codoped oxyfluoride glass ceramic for luminescence thermometry. Journal of Luminescence, 2018, 203, 401-408.	1.5	21

#	Article	IF	CITATIONS
289	Diameter-optimized high-order waveguide nanorods for fluorescence enhancement applied in ultrasensitive bioassays. Nanoscale, 2019, 11, 14322-14329.	2.8	21
290	Continuum theory of 4mm-2mmproper ferroelastic transformation under inhomogeneous stress. Physical Review B, 1990, 42, 4334-4340.	1.1	20
291	<title>Passive materials for high-frequency ultrasound transducers</title> . , 1999, , .		20
292	The elastic and piezoelectric properties of tungsten bronze ferroelectric crystals (Sr0.7Ba0.3)2NaNb5O15 and (Sr0.3Ba0.7)2NaNb5O15. Journal of Applied Physics, 2005, 97, 094106.	1.1	20
293	Thermoelectric Response Driven by Spin-State Transition in La <sub>1â~'<i>x</i></sub> Ce <sub><i>x</i></sub> CoO <sub>3</sub> Perovskites. ACS Applied Materials & Interfaces, 2010, 2, 2213-2217.	4.0	20
294	ZnO Nanorod Array Grown on Ag Layer: A Highly Efficient Fluorescence Enhancement Platform. Scientific Reports, 2015, 5, 8152.	1.6	20
295	Enhanced Energy Storage with Polar Vortices in Ferroelectric Nanocomposites. Physical Review Applied, 2017, 8, .	1.5	20
296	Er3+ doped ferroelectric Pb(Mg1/3Nb2/3)O3–0.25PbTiO3 ceramic used as a linear response fluorescent temperature sensor. Journal of Luminescence, 2017, 181, 128-132.	1.5	20
297	Theoretical study on local domain pinning effect due to defect dipole alignment. Journal Physics D: Applied Physics, 2018, 51, 415303.	1.3	20
298	Improved densification behavior and energy harvesting properties of low-temperature sintered (Ba,) Tj ETQq0 0 C	) rgBT /Ove 2.3	erlock 10 Tf 5
299	Distribution functions of coexisting phases in a complete solid solution system. Journal of Applied Physics, 1993, 73, 3250-3255.	1.1	19
300	Parameter measurement of thin elastic layers using low-frequency multi-mode ultrasonic lamb waves. IEEE Transactions on Instrumentation and Measurement, 2001, 50, 1397-1403.	2.4	19
301	Effective symmetry and physical properties of twinned perovskite ferroelectric single crystals. Journal of Materials Research, 2001, 16, 570-577.	1.2	19
302	Influence of imperfect surface on properties of ferroelectric thin film. Microelectronic Engineering, 2003, 66, 818-824.	1.1	19
303	Acoustic properties of alumina colloidal/polymer nano-composite film on silicon. IEEE Transactions on Ultrasonics, Ferroelectrics, and Frequency Control, 2007, 54, 467-469.	1.7	19
304	Intense red upconversion luminescence from Tm^3+/Yb^3+ codoped transparent glass ceramic. Optics Letters, 2012, 37, 205.	1.7	19
305	Bactericidal effects of hematoporphyrin monomethyl ether-mediated photosensitization against pathogenic communities from supragingival plaque. Applied Microbiology and Biotechnology, 2013, 97, 5079-5087.	1.7	19

#	Article	IF	CITATIONS
307	Hierarchical Assembly of Tungsten Spheres and Epoxy Composites in Three-Dimensional Graphene Foam and Its Enhanced Acoustic Performance as a Backing Material. ACS Applied Materials & Interfaces, 2016, 8, 18496-18504.	4.0	19
308	Doxorubicin combined with low intensity ultrasound suppresses the growth of oral squamous cell carcinoma in culture and in xenografts. Journal of Experimental and Clinical Cancer Research, 2017, 36, 163.	3.5	19
309	Fatigue-free La-modified PbTiO3 thin films prepared by pulsed-laser deposition on Pt/Ti/SiO2/Si substrates. Applied Physics Letters, 2003, 82, 1449-1451.	1.5	18
310	Optical interband transitions in [111] poled relaxor-based ferroelectric 0.24Pb(ln1/2Nb1/2)O3–(0.76Ââ <sup>~^</sup> Âx)Pb(Mg1/3Nb2/3)O3–xPbTiO3 single crystal. Journal of Materials Science, 2012, 47, 2818-2822.	1.7	18
311	Formation Mechanism of (001) Oriented Perovskite SrTiO <sub>3</sub> Microplatelets Synthesized by Topochemical Microcrystal Conversion. Inorganic Chemistry, 2014, 53, 11060-11067.	1.9	18
312	Monochromatic Near-Infrared to Near-Infrared Upconversion Nanoparticles for High-Contrast Fluorescence Imaging. Journal of Physical Chemistry C, 2014, 118, 2820-2825.	1.5	18
313	Dielectric, elastic and piezoelectric properties of SrLaGa3O7 and BaLaGa3O7 crystals with Melilite structure. Journal of Alloys and Compounds, 2015, 647, 1069-1074.	2.8	18
314	Growth and property characterization of CaNdGa <sub>3</sub> O <sub>7</sub> and SrNdGa <sub>3</sub> O <sub>7</sub> melilite single crystals. CrystEngComm, 2015, 17, 1791-1799.	1.3	18
315	Influence of phase transitions on green fluorescence intensity ratio in Er^3+ doped K_05Na_05NbO_3 ceramic. Optics Express, 2016, 24, 29209.	1.7	18
316	Improved fracture behavior and mechanical properties of alumina textured ceramics. Materials Letters, 2018, 221, 252-255.	1.3	18
317	Guided wave propagation in 0.67Pb(Mg1â^•3Nb2â^•3)O3–0.33PbTiO3 single crystal plate poled along [001]c. Applied Physics Letters, 2007, 91, .	1.5	17
318	Experimental investigation on the upconversion mechanism of 754nm NIR luminescence of Ho3+/Yb3+:Y2O3, Gd2O3 under 976nm diode laserexcitation. Journal of Luminescence, 2011, 131, 190-193.	1.5	17
319	Piezoelectric response of charged non-180° domain walls in ferroelectric ceramics. Journal of Applied Physics, 2012, 111, 024106.	1.1	17
320	Structural Evolving Sequence and Porous <scp><scp>Ba</scp></scp> <sub>6</sub> <scp>Zr</scp> 2 <scp><scp>Nb</scp></scp> Ferroelectric Ceramics with Ultrahigh Breakdown Field and Zero Strain. Journal of the American Ceramic Society, 2013, 96, 555-560.	<sub>81.9</sub>	sub> < scp> <
321	Mechanism of Gadolinium Doping Induced Room-Temperature Phosphorescence from Porphyrin. Journal of Physical Chemistry C, 2015, 119, 10558-10563.	1.5	17
322	Temperature dependence of dielectric, elastic, and piezoelectric constants of [001]c poled Mn-doped 0.24Pb(In1/2Nb1/2)O3-0.46Pb(Mg1/3Nb2/3)O3-0.30PbTiO3 single crystal. Applied Physics Letters, 2016, 108, 082901.	1.5	17
323	Small molecule inhibitor of c-Met (PHA665752) suppresses the growth of ovarian cancer cells and reverses cisplatin resistance. Tumor Biology, 2016, 37, 7843-7852.	0.8	17
324	High-Frequency Ultrasonic Imaging with Lead-free (Na,K)(Nb,Ta)O <sub>3</sub> Single Crystal. Ultrasonic Imaging, 2017, 39, 348-356.	1.4	17

#	Article	IF	CITATIONS
325	Enhanced electric field induced strain in (1-x)((Bi0.5Na0.5)TiO3-Ba(Ti, Zr)O3)-xSrTiO3 ceramics. Ceramics International, 2018, 44, 12869-12876.	2.3	17
326	Temperature dependence of third-order elastic constants of potassium manganese fluoride. Physical Review B, 1988, 38, 10244-10255.	1.1	16
327	Development and evaluation of the polymerase chain reaction method for diagnosis of Mycoplasma gallisepticum infection in chickens. Molecular and Cellular Probes, 1993, 7, 459-463.	0.9	16
328	Finite Element Analysis and Experimental Studies on the Thickness Resonance of Piezocomposite Transducers. Ultrasonic Imaging, 1996, 18, 1-9.	1.4	16
329	Effect of grain size on actuator properties of piezoelectric ceramics. , 1998, , .		16
330	High frequency permittivity determination by spectra simulation and measurement of microstrip ring resonators. Electronics Letters, 2000, 36, 956.	0.5	16
331	Determination of full set material constants of piezoceramics from phase velocities. Journal of Applied Physics, 2002, 92, 4578-4583.	1.1	16
332	High-frequency dispersion of ultrasonic velocity and attenuation of single-crystal 0.72 Pb(Mg1/3Nb2/3)O3–0.28 PbTiO3 with engineered domain structures. Applied Physics Letters, 2 2466-2468.	002580,	16
333	Switching Mechanism in Single Crystal 0.955Pb(Zn 1/3 Nb 2/3 )O 3 -0.045PbTiO 3. Ferroelectrics, 2003, 290, 107-114.	0.3	16
334	Piezoelectric properties of domain engineered barium titanate single crystals with different volume fractions of domain walls. Journal of Applied Physics, 2009, 106, 064102.	1.1	16
335	Theoretical study on guided wave propagation in (1) Tj ETQq1 1 0.784314 rgBT /Overlock 10 Tf 50 347 Td (â^' <i></i>	•x)Pb(I 1.3	Mg <sub>1/3 16</sub>
336	Modeling of board-level package by Finite Element Analysis and laser interferometer measurements. Microelectronics Reliability, 2010, 50, 1021-1027.	0.9	16
337	Effect of Eu3 + codoping on upconversion luminescence in Y2O3:Er3 +, Yb3 + nanocrystals. Solid State Communications, 2010, 150, 1048-1051.	0.9	16
338	Domain evolution with electric field and delineation of extrinsic contributions in (K, Na, Li)(Nb, Ta,) Tj ETQq0 0 0 r	gBT_/Over	lock 10 Tf 50
339	Effect of kerf filler on the electromechanical coupling coefficient of 1–3 piezoelectric composites. Journal of Alloys and Compounds, 2015, 651, 643-647.	2.8	16

xmlns:mml="http://www.w3.org/1998/Math/MathML"><mml:msub><mml:mi mathvariant="normal">M</mml:mi><mml:mi>C</mml:mi></mml:msub></mml:math>phase in<mml:math 340

#	Article	IF	CITATIONS
343	Tetragonal (K, Na)NbO3 based lead-free single crystal: Growth, full tensor properties, and their orientation dependence. Applied Physics Letters, 2017, 111, .	1.5	16
344	Enhancing the Temperature Stability of 0.42PNN-0.21PZ-0.37PT Ceramics through Texture Engineering. ACS Applied Materials & Interfaces, 2022, 14, 3076-3083.	4.0	16
345	Dielectric anomalies in [111] oriented 0.955Pb(Zn1/3Nb2/3)O3â^0.045PbTiO3 single crystals under different electrical and thermal conditions. Journal of Applied Physics, 2004, 95, 8124-8129.	1.1	15
346	Phase transition and ferroelectric properties of epitaxially strained KNbO3/NaNbO3 superlattice. Journal of Applied Physics, 2008, 104, 126106.	1.1	15
347	Theoretical and Experimental Study on Temperature Elevation behind Ribs Caused by Weakly Focused Ultrasound in Medicine and Biology, 2010, 36, 1704-1712.	0.7	15
348	Linear electro-optic properties of relaxor-based ferroelectric 0.24Pb(In1/2Nb1/2)O3-(0.76 â~' <i>x</i> )Pb(Mg1/3Nb2/3)O3- <i>x</i> PbTiO3 single crystals. Journal of Physics, 2013, 114, 27021.	Applied	15
349	Twenty-fold Enhancement of Gadolinium-Porphyrin Phosphorescence at Room Temperature by Free Gadolinium Ion in Liquid Phase. Journal of Physical Chemistry C, 2015, 119, 28111-28116.	1.5	15
350	Electric field induced upconversion fluorescence enhancement and its mechanism in Er3+ doped 0.75Pb(Mg1/3Nb2/3)O3-0.25PbTiO3 transparent ceramic. Applied Physics Letters, 2016, 109, .	1.5	15
351	Improved depolarization behavior and electric properties in (Bi0.5Na0.5)TiO3-based piezoelectric composites. Journal of Alloys and Compounds, 2018, 769, 660-668.	2.8	15
352	Dynamic scaling of internal bias field in Mn-doped 0.24Pb(In1/2Nb1/2)O3–0.42Pb(Mg1/3Nb2/3)O3–0.34PbTiO3 ferroelectric ceramic. Journal of Materials Science, 2018, 53, 12762-12769.	1.7	15
353	NIR to NIR luminescence thermometry in core/multishells-structured nanoparticles operating in the biological window. Journal of Luminescence, 2020, 225, 117358.	1.5	15
354	Scaling relations of domain reversal dynamics in rhombohedral and tetragonal PIN–PMN–PT ferroelectric single crystals. Applied Physics Letters, 2021, 119, .	1.5	15
355	Theory on the fringe patterns in the study of ferroelectric domain walls using electron holography. Solid State Communications, 1993, 86, 435-439.	0.9	14
356	Microstructural characteristics and diffuse phase transition behavior of lanthanum-modified lead titanate. Ferroelectrics, 1994, 158, 343-350.	0.3	14
357	Polarization Gradient Coefficients and the Dispersion Surface of the Soft Mode in Perovskite Ferroelectrics. Journal of the Physical Society of Japan, 1994, 63, 1156-1161.	0.7	14
358	Electromechanical coupling coefficient of 0.70Pb(Mg1â^•3Nb2â^•3)O3–0.30PbTiO3 single crystal resonator with arbitrary aspect ratio. Applied Physics Letters, 2007, 91, 122903.	1.5	14
359	Complete set of material properties of [011]c poled 0.24Pb(ln1/2Nb1/2)O3–0.46Pb(Mg1/3Nb2/3)O3–0.30PbTiO3 single crystal. Materials Letters, 2011, 65, 2855-2857.	1.3	14
360	Enhancing upconversion emissions of NaTm0.02YbxY0.98â^'xF4 nanocrystals through increasing Yb3+ doping. Journal of Luminescence, 2011, 131, 1802-1806.	1.5	14

#	Article	IF	CITATIONS
361	Investigation on upconversion photoluminescence of Bi3TiNbO9:Er3+:Yb3+ thin films. Journal of Luminescence, 2011, 131, 2574-2578.	1.5	14
362	Shell thickness dependence of upconversion luminescence of β-NaYF_4:Yb, Er/β-NaYF_4 core-shell nanocrystals. Optics Letters, 2013, 38, 2101.	1.7	14
363	Theoretical study on phase coexistence in ferroelectric solid solutions near the tricritical point. Journal of Applied Physics, 2015, 117, 134101.	1.1	14
364	Growth and characterization of lead-free ferroelectric (K,Na,Li)(Nb,Ta,Sb)O3 single crystal. Journal of Crystal Growth, 2015, 409, 39-43.	0.7	14
365	Topochemical transformation of single crystalline SrTiO <sub>3</sub> microplatelets from Bi <sub>4</sub> Ti <sub>3</sub> O <sub>12</sub> precursors and their orientation-dependent surface piezoelectricity. CrystEngComm, 2018, 20, 3084-3095.	1.3	14
366	Parameters identification and contact analysis of traveling wave ultrasonic motor based on measured force and feedback voltage. Sensors and Actuators A: Physical, 2018, 284, 201-208.	2.0	14
367	Bactericidal effects of hematoporphyrin monomethyl ether-mediated blue-light photodynamic therapy against Staphylococcus aureus. Photochemical and Photobiological Sciences, 2019, 18, 92-97.	1.6	14
368	Improved ultrasonic spectroscopy methods for characterization of dispersive materials. IEEE Transactions on Ultrasonics, Ferroelectrics, and Frequency Control, 2001, 48, 1060-1065.	1.7	13
369	Electronic band-structure engineering of GaAs/AlxGa1â^'xAs quantum well superlattices with substructures. Materials Science and Engineering B: Solid-State Materials for Advanced Technology, 2003, 103, 122-127.	1.7	13
370	Electric-field-induced dielectric anomalies in C-oriented 0.955Pb(Zn1/3Nb2/3)O3–0.045PbTiO3 single crystals. Applied Physics Letters, 2003, 83, 731-733.	1.5	13
371	Preparation and characterization of transparent PZN–PLZT ceramics. Journal of Materials Research, 2004, 19, 729-732.	1.2	13
372	Characterizing ultra-thin matching layers of high-frequency ultrasonic transducer based on impedance matching principle. IEEE Transactions on Ultrasonics, Ferroelectrics, and Frequency Control, 2004, 51, 211-215.	1.7	13
373	Valley-to-peak intensity ratio thermometry based on the red upconversion emission of Er^3+. Optics Express, 2016, 24, 13244.	1.7	13
374	Growth and property enhancement of Er 3+ -doped 0.68Pb(Mg 1/3 Nb 2/3 )O 3 -0.32PbTiO 3 single crystal. Journal of Rare Earths, 2018, 36, 832-837.	2.5	13
375	Magnesium Alloy Matching Layer for High-Performance Transducer Applications. Sensors, 2018, 18, 4424.	2.1	13
376	Large photovoltaic effect with ultrahigh open-circuit voltage in relaxor-based ferroelectric Pb(ln1/2Nb1/2)O3-Pb(Mg1/3Nb2/3)O3-PbTiO3 ceramics. Journal of Materials Science and Technology, 2022, 104, 119-126.	5.6	13
377	Finite element analysis of periodic and random 2-2 piezocomposite transducers with finite dimensions. IEEE Transactions on Ultrasonics, Ferroelectrics, and Frequency Control, 1997, 44, 1168-1171.	1.7	12
378	Electromechanical properties of thin strip piezoelectric vibrators at high frequency. Journal of Applied Physics, 2000, 88, 394-397.	1.1	12

#	Article	IF	CITATIONS
379	Landau-Ginzburg model for antiferroelectric phase transitions based on microscopic symmetry. Physical Review B, 2000, 62, 818-823.	1.1	12
380	Analysis of resonance processes in microstrip ring resonators by the FDTD method. Microwave and Optical Technology Letters, 2001, 28, 312-321.	0.9	12
381	Structural, dielectric and optical properties of barium strontium sodium niobate (Sr0.7Ba0.3)2NaNb5O15single crystals. Journal Physics D: Applied Physics, 2004, 37, 921-924.	1.3	12
382	Optical properties of highly C-oriented Bi3TiNbO9 thin films grown on fused silica substrates by PLD. Applied Physics A: Materials Science and Processing, 2005, 81, 183-186.	1.1	12
383	Contributions of domain wall motion to complex electromechanical coefficients of 0.62Pb(Mg1/3Nb2/3)O3–0.38PbTiO3 crystals. Journal of Applied Physics, 2010, 107, 14110.	1.1	12
384	Apoptosis of vascular smooth muscle cells induced by photodynamic therapy with protoporphyrin IX. Biochemical and Biophysical Research Communications, 2010, 391, 69-72.	1.0	12
385	Reduction of electro-optic half-wave voltage of 0.93Pb(Zn1/3Nb2/3)O3–0.07PbTiO3 single crystal through large piezoelectric strain. Optical Materials, 2011, 33, 549-552.	1.7	12
386	Switching 70Pb(Mg1/3Nb2/3)O3-0.30PbTiO3 single crystal by 3 MHz bipolar field. Applied Physics Letters, 2016, 108, 232901.	1.5	12
387	Facile synthesis and upconversion luminescence of β-NaYF4:Yb, Tm nanocrystals with highly tunable and uniform β-NaYF4 shells. Journal of Alloys and Compounds, 2016, 684, 211-216.	2.8	12
388	40% enhanced photocurrent of dye sensitized solar cells using lotus-shaped H 2 -treated anatase TiO 2 with {0 0 1} dominated facets. Chemical Engineering Journal, 2017, 316, 534-543.	6.6	12
389	Determination of temperature dependence of full matrix material constants of PZT-8 piezoceramics using only one sample. Journal of Alloys and Compounds, 2017, 714, 20-25.	2.8	12
390	Single-Crystal High-Frequency Intravascular Ultrasound Transducer With 40-\$mu\$ m Axial Resolution. IEEE Transactions on Ultrasonics, Ferroelectrics, and Frequency Control, 2020, 67, 810-816.	1.7	12
391	Nonlinear and nonlocal continuum theory on domain walls in ferroelectrics. Ferroelectrics, 1994, 157, 19-26.	0.3	11
392	Effects of face plates on surface displacement profile in 2-2 piezoelectric composites. IEEE Transactions on Ultrasonics, Ferroelectrics, and Frequency Control, 1995, 42, 37-41.	1.7	11
393	Direct measurement of ultrasonic velocity of thin elastic layers. Journal of the Acoustical Society of America, 1997, 101, 626-628.	0.5	11
394	Temperature-dependence of carbon film growth by electrolysis of a methanol solution. Carbon, 2003, 41, 594-598.	5.4	11
395	Influence of imperfect surface layers on dielectric and pyroelectric properties of ferroelectric thin film. Physica B: Condensed Matter, 2006, 373, 177-181.	1.3	11
396	Surface acoustic wave propagation properties in 0.67Pb(Mg1/3Nb2/3)O3-0.33PbTiO3 single crystal poled along [111]c. Applied Physics Letters, 2009, 95, 242906.	1.5	11

#	Article	IF	CITATIONS
397	Polarized Raman study on phase transitions in 0.24Pb(In1/2Nb1/2)O3–0.43Pb(Mg1/3Nb2/3)O3–0.33PbTiO3 single crystal. Journal of Alloys and Compounds, 2013, 551, 98-100.	2.8	11
398	<sup>3</sup> Upconversion emission efficiency of Tb^3+-Yb^3+ codoped glass. Journal of the Optical Society of America B: Optical Physics, 2013, 30, 456.	0.9	11
399	Synthesis and properties of high aspect ratio SrBi4Ti4O15 microplatelets. Materials Letters, 2014, 129, 126-129.	1.3	11
40	Mechanism of rat osteosarcoma cell apoptosis induced by a combination of low-intensity ultrasound and 5-aminolevulinic acid in vitro. Genetics and Molecular Research, 2015, 14, 9604-9613.	0.3	11
40	Graphene oxide-stimulated acoustic attenuating performance of tungsten based epoxy films. Journal of Materials Chemistry C, 2015, 3, 10848-10855.	2.7	11
40	Decatungstate acid improves the photo-induced electron lifetime and retards the recombination in dye sensitized solar cells. Dalton Transactions, 2016, 45, 14940-14947.	1.6	11
40	Photophysical properties of sinoporphyrin sodium and explanation of its high photo-activity. Journal of Porphyrins and Phthalocyanines, 2017, 21, 59-66.	0.4	11
404	Ratiometric oxygen sensing using the tunable ratio of phosphorescence to fluorescence emissions from gadolinium porphyrin and porphyrin. Journal of Luminescence, 2017, 183, 452-457.	1.5	11
40	Vertical MoSe <sub>2</sub> –MoO <i> <sub>x</sub> </i> p–n heterojunction and its application in optoelectronics. Nanotechnology, 2018, 29, 045202.	1.3	11
40	Dynamic characteristics of defect dipoles in Mn-doped 0.24Pb(In <sub>1/2</sub> Nb <sub>1/2</sub> )O <sub>3</sub> –0.47Pb(Mg <sub>1/3</sub> Nb <sub>2/3</sub> ) single crystal. CrystEngComm, 2019, 21, 348-355.	)Otæub>	3 ∎sub –0
40'	Effects of palmatine hydrochloride mediated photodynamic therapy on oral squamous cell carcinoma. Photochemical and Photobiological Sciences, 2019, 18, 1596-1605.	1.6	11
40	8 Defect stabilized periodic amplitude modulations in ferroelectrics. Phase Transitions, 1995, 55, 69-78.	0.6	10
40	<ul> <li>Modeling of microwave ring resonators using the finite-difference time-domain method (FDTD).</li> <li>Microwave and Optical Technology Letters, 2000, 24, 392-396.</li> </ul>	0.9	10
410	Influence of sample size on ultrasonic phase velocity measurements in piezoelectric ceramics. Journal of Applied Physics, 2002, 91, 10194.	1.1	10
411	Highly confined energy propagation in a gap waveguide composed of two coupled nanorod chains. Applied Physics Letters, 2007, 91, 133107.	1.5	10
412	Poling field versus piezoelectric property for [001] c oriented 91%Pb(Zn1/3Nb2/3)O3–9%PbTiO3 single crystals. Journal of Materials Science, 2011, 46, 1839-1843.	1.7	10
413	Ultraviolet upconversion luminescence of Gd3+ from Ho3+ and Gd3+ codoped oxide ceramic induced by 532-nm CW laser excitation. Optics Communications, 2011, 284, 3114-3117.	1.0	10
414	Current-voltage characteristics and ON/OFF ratio in ferroelectric tunnel junctions. Journal of Applied Physics, 2012, 112, 054102.	1.1	10

#	Article	IF	CITATIONS
415	Absolute quantum cutting efficiency of Tb3+-Yb3+ co-doped glass. Journal of Applied Physics, 2013, 114, 213513.	1.1	10
416	Electrical behaviors of c-axis textured 0.975Bi0.5Na0.5TiO3–0.025BiCoO3 thin films grown by pulsed laser deposition. Applied Surface Science, 2013, 283, 759-763.	3.1	10
417	Enhanced Electrical Properties of Novel Pb(Ni <sub>1/3</sub> Nb <sub>2/3</sub> )O <sub>3</sub> –BiScO <sub>3</sub> –PbTiO <sub>3</sub> Ternary System near Morphotropic Phase Boundary. Japanese Journal of Applied Physics, 2013, 52, 101101.	0.8	10
418	Low-Intensity Ultrasound Combined with Hematoporphyrin Monomethyl Ether in the Treatment of Experimental Periodontitis in Rats. BioMed Research International, 2016, 2016, 1-6.	0.9	10
419	Quantitative lateral and vertical piezoresponse force microscopy on a PbTiO3 single crystal. Journal of Applied Physics, 2016, 120, 124106.	1.1	10
420	Phase coexistence in ferroelectric solid solutions: Formation of monoclinic phase with enhanced piezoelectricity. AIP Advances, 2016, 6, .	0.6	10
421	Optical bandgap and dispersions of 0.24Pb(In 1/2 Nb 1/2 )O 3 -0.43Pb(Mg 1/3 Nb 2/3 )O 3 -0.33PbTiO 3 single crystal poled along [011] c direction. Optical Materials, 2016, 60, 101-104.	1.7	10
422	Protoporphyrin IX-mediated sonodynamic therapy promotes autophagy in vascular smooth muscle cells. Oncology Letters, 2017, 14, 2097-2102.	0.8	10
423	Comprehensive analysis of Mn:PIN-PMN-PT single crystals for Class IV flextensional transducer. Ceramics International, 2018, 44, 2864-2868.	2.3	10
424	Sonodynamic therapy improves anti‑tumor immune effect by increasing the infiltration of CD8+ T cells and altering tumor blood vessels in murine B16F10 melanoma xenograft. Oncology Reports, 2018, 40, 2163-2170.	1.2	10
425	Evaluation of reversible and irreversible domain wall motions in relaxor ferroelectrics: Influence of acceptor ions. Applied Physics Letters, 2019, 114, .	1.5	10
426	Finite Element Analysis and Experimental Studies on the Thickness Resonance of Piezocomposite Transducers. Ultrasonic Imaging, 1996, 18, 1-9.	1.4	9
427	<title>Determination of elastic, piezoelectric, and dielectric properties of&lt;br&gt;Pb(Zn&lt;formula&gt;&lt;inf&gt;&lt;roman&gt;1/3&lt;/roman&gt;&lt;/inf&gt;&lt;/formula&gt;Nb&lt;formula&gt;&lt;inf&gt;&lt;roman&gt;2/3&lt;/roman&gt;&lt;/inf&gt;&lt;/form&lt;br&gt;single crystals</title> ., 1999, 3664, 239.	ıula>)O <f< td=""><td>o<b>e</b>mula&gt;<in< td=""></in<></td></f<>	o <b>e</b> mula> <in< td=""></in<>
428	Allowed mesoscopic point group symmetries in domain average engineering of perovskite ferroelectric crystals. Journal of Applied Physics, 2003, 94, 5220.	1.1	9
429	Frequency dispersion of ultrasonic velocity and attenuation of longitudinal waves propagating in 0.68Pb(Mg1â^•3Nb2â^•3)O3–0.32PbTiO3 single crystals poled along [001] and [110]. Applied Physics Letters, 2005, 87, 182903.	1.5	9
430	Surface acoustic wave propagation in Y- and Z-cut 0.67PbMgNbO3–0.33PbTiO3 single crystals. Journal of Applied Physics, 2009, 106, 054110.	1.1	9
431	Electromechanical coupling coefficient k31eff for arbitrary aspect ratio resonators made of [001] and [011] poled (1Ⱂx)Pb(Mg1/3Nb2/3)O3–xPbTiO3 single crystals. Journal of Applied Physics, 2009, 105, 064104.	1.1	9
432	Nonlinear restoring forces and geometry influence on stability in near-field acoustic levitation. Journal of Applied Physics, 2011, 109, .	1.1	9

#	Article	IF	CITATIONS
433	Phase Transition and Electrical Properties of <scp><scp>Ba</scp></scp> <sub>0.7</sub> <scp><a< scp="">0.3<scp>TiO</scp><!--<br-->Ceramics. Journal of the American Ceramic Society, 2012, 95, 3901-3905.</a<></scp>	s¢p> <sut< td=""><td>o&gt;9â</td></sut<>	o>9â
434	Optical properties and dispersions of rhombohedral 0.24Pb(ln1/2Nb1/2)O3–0.49Pb(Mg1/3Nb2/3)O3–0.27PbTiO3 single domain single crystal. Optical Materials, 2013, 36, 342-345.	1.7	9
435	Determination of full set material constants of [011]c poled 0.72Pb(Mg1/3Nb2/3)O3-0.28PbTiO3 single crystal from one sample. Applied Physics Letters, 2014, 105, 012901.	1.5	9
436	Arrays of nanorods composed of ZnO nanodots exhibiting enhanced UV emission and stability. Nanoscale, 2014, 6, 10746-10751.	2.8	9
437	A single-mode Mn-doped 0.27PIN-0.46PMN-0.27PT single-crystal ultrasonic motor. Journal of Flectroceramics, 2016, 37, 121-126 Landau expansion parameters and the <i>O-T</i> phase transition of a <mml:math< td=""><td>0.8</td><td>9</td></mml:math<>	0.8	9

#	Article	IF	CITATIONS
451	Controlling the angle range in acoustic low-frequency forbidden transmission in solid-fluid superlattice. Journal of Applied Physics, 2018, 123, .	1.1	8
452	Magnesium Alloy Matching Layer for PMN-PT Single Crystal Transducer Applications. IEEE Transactions on Ultrasonics, Ferroelectrics, and Frequency Control, 2018, 65, 1865-1872.	1.7	8
453	Potential involvement of the 18 kDa translocator protein and reactive oxygen species in apoptosis of THP-1 macrophages induced by sonodynamic therapy. PLoS ONE, 2018, 13, e0196541.	1.1	8
454	Modeling dynamic rotation of defect dipoles and poling time dependence of piezoelectric effect in ferroelectrics. Applied Physics Letters, 2019, 114, .	1.5	8
455	Temperature- and frequency-dependent hysteresis scaling behaviour and phase transitions in a [001]c 0.73Pb(Mg1/3Nb2/3)O3-0.27PbTiO3 single crystal. Ceramics International, 2020, 46, 8675-8681.	2.3	8
456	Dielectric, elastic and piezoelectric properties of single domain Pb(Zn1/3Nb2/3)O3–6.5%PbTiO3 single crystal with 3m symmetry measured using one sample. Scripta Materialia, 2021, 194, 113634.	2.6	8
457	Sonodynamic Effects of a Novel Ether-Group Modified Porphyrin Derivative Combined With Pulsed Low-Intensity Ultrasound on PC-9 Cells. Frontiers in Pharmacology, 2021, 12, 792360.	1.6	8
458	Ultrahigh strain in textured BCZT-based lead-free ceramics with CuO sintering agent. Journal of Materials Science and Technology, 2022, 117, 207-214.	5.6	8
459	Periodic superstructures in tetrahedrally bonded homopolymers. Physical Review B, 1988, 38, 7664-7673.	1.1	7
460	Antiphase structures of an improper ferroelastic phase transition driven by anM5â^'zone boundary phonon inRAg1â^'xInx. Physical Review B, 2001, 64, .	1.1	7
461	Combining FDTD simulations with measurements of microstrip ring resonators for characterization of low- and high-K dielectrics at microwaves. Microwave and Optical Technology Letters, 2001, 29, 21-24.	0.9	7
462	Theoretical study on the influence of surface imperfections on the properties of ferroelectric thin films in first-order ferroelectric systems. Physica Status Solidi (B): Basic Research, 2006, 243, 2952-2961.	0.7	7
463	Experimental technique for characterizing arbitrary aspect ratio piezoelectric resonators. Applied Physics Letters, 2006, 89, 162910.	1.5	7
464	Optical properties of Bi2.25La0.75TiNbO9 thin films grown on fused silica substrates by PLD. Optical Materials, 2009, 32, 406-409.	1.7	7
465	Frequency dispersion of longitudinal ultrasonic velocity and attenuation in [001]c-poled 0.24Pb(In1/2Nb1/2)O3- 0.45Pb(Mg1/3Nb2/3)O3-0.31PbTiO3Single Crystal. IEEE Transactions on Ultrasonics, Ferroelectrics, and Frequency Control, 2011, 58, 1669-1673.	1.7	7
466	Ultraviolet emissions from Gd3+ ions excited by energy transfer from Ho3+ ions. Journal of Luminescence, 2011, 131, 347-351.	1.5	7
467	Three Dimensional Domain Structures for Domain Engineered Rhombohedral Perovskite Ferroelectric Crystals. Ferroelectrics, 2012, 426, 13-20.	0.3	7
468	Converse-piezoelectric effect on current-voltage characteristics of symmetric ferroelectric tunnel junctions. Journal of Applied Physics, 2012, 111, .	1.1	7

#	Article	lF	CITATIONS
469	High sensitivity gravimetric sensor made of carbon fiber epoxy composite on Pb(Mg1/3Nb2/3)O3-PbTiO3single crystal substrate. Applied Physics Letters, 2013, 103, 053507.	1.5	7
470	Effect of cell cycle phase on the sensitivity of SAS cells to sonodynamic therapy using low-intensity ultrasound combined with 5-aminolevulinic acid in vitro. Molecular Medicine Reports, 2015, 12, 3177-3183.	1.1	7
471	The effect of polymeric filler on poling behavior and thermal stability of 1-3 piezoelectric composites. Journal Physics D: Applied Physics, 2016, 49, 025301.	1.3	7
472	Effect of misfit strain on ferroelectric domain formation at the morphotropic phase boundary. Physical Review B, 2016, 94, .	1.1	7
473	Prolonged lifetime and retarded recombination inÂdye sensitized solar cells using hydrogenated fluorine doped TiO <sub>2</sub> nanocrystals as a photoanode. RSC Advances, 2016, 6, 99251-99259.	1.7	7
474	The effect of imidazole on the enhancement of gadolinium-porphyrin phosphorescence at room temperature. Dalton Transactions, 2016, 45, 16889-16895.	1.6	7
475	Effect of annealing temperature on the optical property of high Cd content CdZnO films. Superlattices and Microstructures, 2016, 97, 569-574.	1.4	7
476	Depoling and fatigue behavior of Pb(Mg1/3Nb2/3)O3-PbTiO3 single crystal at megahertz frequencies under bipolar electric field. Journal of Applied Physics, 2017, 121, 174101.	1.1	7
477	The effect of annealing temperature on the optical and electrical properties of cubic MgZnO films grown by RF magnetron sputtering. Journal of Materials Science: Materials in Electronics, 2017, 28, 1644-1651.	1.1	7
478	A subwavelength asymmetric acoustic design for waveform-preserved highly forward transmission. AIP Advances, 2018, 8, 085102.	0.6	7
479	Detecting trace of mercury ions in water using photoacoustic method enhanced by gold nanospheres. Microchemical Journal, 2019, 150, 104058.	2.3	7
480	Temperature-dependent phase transition in [001]-oriented 0.72Pb(MgNb)O-0.28PbTiO single crystals. Ceramics International, 2019, 45, 13999-14005.	2.3	7
481	Dielectric relaxation properties of [001] <sub>c</sub> â€; [011] <sub>c</sub> â€; and [111] <sub>c</sub> â€oriented 0.24PINâ€0.47PMNâ€0.29PT single crystals. Journal of the American Ceramic Society, 2019, 102, 4103-4112.	1.9	7
482	Dielectric relaxation and local domain structures of ferroelectric PIMNT and PMNT single crystals. Journal of the American Ceramic Society, 2020, 103, 1744-1754.	1.9	7
483	Tonpilz transducer head mass selection based on excitation signal type. Applied Acoustics, 2021, 176, 107852.	1.7	7
484	Self-heating phenomenon of piezoelectric elements excited by a tone-burst electric field. Ultrasonics, 2021, 117, 106562.	2.1	7
485	Defects in Ferroelectrics. Springer Series in Materials Science, 2012, , 113-134.	0.4	7
486	Elimination of pyrochlore phase in highâ€concentration Sm <sup>3+</sup> â€doped PMNâ€PT piezoelectric ceramics by excessive MgO. Journal of the American Ceramic Society, 2022, 105, 4180-4190.	1.9	7

#	Article	IF	CITATIONS
487	Multisource excitations in a stratified biphase structure. Journal of Applied Physics, 1995, 78, 4640-4646.	1.1	6
488	Observation and analysis of domain configurations in domain engineered PZN-PT single crystals. Ferroelectrics, 2001, 251, 93-100.	0.3	6
489	Computer simulations of domain pattern formation in ferroelectrics. AIP Conference Proceedings, 2001, , .	0.3	6
490	Phenomenological theories of ferroelectric phase transitions. Advances in Applied Ceramics, 2004, 103, 71-75.	0.4	6
491	Second harmonic generation of shear waves in crystals. IEEE Transactions on Ultrasonics, Ferroelectrics, and Frequency Control, 2004, 51, 153-162.	1.7	6
492	Effect of kerf filler on the electromechanical coupling coefficient of an ultrasonic transducer array element. Applied Physics Letters, 2007, 91, .	1.5	6
493	Aspect Ratio Dependence of Electromechanical Coupling Coefficient k <sub>31</sub> of Lateral-Excitation Piezoelectric Vibrator. Japanese Journal of Applied Physics, 2007, 46, 4459.	0.8	6
494	Dielectric properties of ferroelectric thin films with surface transition layers. Physica A: Statistical Mechanics and Its Applications, 2008, 387, 1963-1971.	1.2	6
495	Dielectric and piezoelectric properties of sodium lithium niobate Na1â^x Li x NbO3 lead free ferroelectric ceramics. Journal of Electroceramics, 2008, 21, 323-326.	0.8	6
496	Pressure-sensitive blackbody point radiation induced by infrared diode laser irradiation. Optics Letters, 2011, 36, 1806.	1.7	6
497	Pressure tuned ferroelectric reentrance in nano-BaTiO3 ceramics. Journal of Applied Physics, 2012, 112,	1.1	6
498	A quantitative diagnostic method for oral mucous precancerosis by Rose Bengal fluorescence spectroscopy. Lasers in Medical Science, 2013, 28, 241-246.	1.0	6
499	Labeling efficiency and toxicity evaluation of CdSe/ZnS quantum dots on Escherichia coli. Journal of Nanoparticle Research, 2014, 16, 1.	0.8	6
500	Acoustic beam control in biomimetic projector via velocity gradient. Applied Physics Letters, 2016, 109,	1.5	6
501	Fluorescence intensity ratio thermometer methodology of eliminating the "decoupling―effect of a pair of thermally coupled energy levels of rare-earth ions. Optics Letters, 2017, 42, 1401.	1.7	6
502	Domain engineering and full matrix material constants of the [111] <sub>c</sub> -poled 0.63Pb(Mg <sub>1/3</sub> Nb <sub>2/3</sub> )-0.37PbTiO <sub>3</sub> single crystal. CrystEngComm, 2018, 20, 4745-4751.	1.3	6
503	Ferroelectric fatigue and polarization hysteresis behavior of a [001]c Pb(In0.5Nb0.5)O3-Pb(Mg1/3Nb2/3)O3-PbTiO3 single crystal. Journal of Materials Science, 2021, 56, 9655-9667.	1.7	6
504	Lead-Free Ultrasonic Phased Array Transducer for Human Heart Imaging. IEEE Transactions on Ultrasonics, Ferroelectrics, and Frequency Control, 2022, 69, 751-760.	1.7	6

#	Article	IF	CITATIONS
505	Hematoporphyrin monomethyl etherâ€ʿmediated sonodynamic therapy induces Aâ€ʿ253 cell apoptosis. Oncology Letters, 2020, 19, 3223-3228.	0.8	6
506	Intrinsic and coupling-induced elastic nonlinearity of lanthanum-doped lead magnesium niobate–lead titanate electrostrictive ceramic. Applied Physics Letters, 2000, 77, 1387-1389.	1.5	5
507	Improving leakage currents of Pt/Ba0.8Sr0.2TiO3/Pt capacitors using multilayered structures. Surface and Coatings Technology, 2002, 160, 277-281.	2.2	5
508	Pulsed laser deposition optical waveguiding Bi3TiNbO9 thin films on fused silica. Thin Solid Films, 2005, 473, 296-299.	0.8	5
509	Dielectric enhancement in interface-modified BaTiO3/SrTiO3 multilayered films prepared by pulsed laser deposition. Microelectronic Engineering, 2006, 83, 553-556.	1.1	5
510	Investigation of dipolar defects in (1â^'x)Pb(Zn1â^•3Nb2â^•3)O3–xPbTiO3 single crystals using different poling methods. Journal of Applied Physics, 2007, 101, 014105.	1.1	5
511	Nonlinear optical absorption in Bi3TiNbO9 thin films using Z-scanÂtechnique. Applied Physics A: Materials Science and Processing, 2009, 96, 1017-1021.	1.1	5
512	Surface Acoustic Wave Propagation in Relaxor-Based Ferroelectric Single Crystals 0.93Pb(Zn 1/3 Nb 2/3) Tj ETQq(	) 0 0 rgBT 1.3	/Gverlock 10
513	Theoretical study on piezoresponse of ultrathin ferroelectric films. Journal of Applied Physics, 2012, 112, 074115.	1.1	5
514	Space charge effect in ultrathin ferroelectric films. Journal of Applied Physics, 2012, 111, 084103.	1.1	5
515	A nonlinear model for the layer between plates in acoustic noncontact transportation. Journal of Applied Physics, 2014, 116, .	1.1	5
516	Characterizing full matrix constants of piezoelectric single crystals with strong anisotropy using two samples. Journal of Applied Physics, 2016, 120, .	1.1	5
517	Characterization of Full Set Material Constants and Their Temperature Dependence for Piezoelectric Materials Using Resonant Ultrasound Spectroscopy. Journal of Visualized Experiments, 2016, , .	0.2	5
518	Nonlinear phosphorescence quenching mechanism of gadolinium labeled porphyrin by oxygen on filter paper. Journal of Photochemistry and Photobiology A: Chemistry, 2016, 316, 7-11.	2.0	5
519	Influence of Finite Size on the Electrocaloric Response in PbTiO <sub>3</sub> Ceramics Near Room Temperature Using Landau Theory. Physica Status Solidi (B): Basic Research, 2018, 255, 1700469.	0.7	5
520	Effects of low-intensity ultrasound combined with low-dose carboplatin in an orthotopic hamster model of tongue cancer: A preclinical study. Oncology Reports, 2018, 39, 1609-1618.	1.2	5
521	Morphology-controlled synthesis of α-alumina microplatelets through an additive-assisted molten salt reaction. Materials Letters, 2018, 210, 182-185.	1.3	5
522	Low-frequency forbidden bandgap engineering via a cascade of multiple 1D superlattices. Journal of Applied Physics, 2018, 124, 155102.	1.1	5

#	Article	IF	CITATIONS
523	Temperature dependent piezoelectric anisotropy in tetragonal 0.63Pb(Mg1/3Nb2/3)-0.37PbTiO3 single crystal. Applied Physics Letters, 2018, 113, 102903.	1.5	5
524	Defect dynamics in clusters of self-propelled rods in circular confinement. European Physical Journal E, 2019, 42, 150.	0.7	5
525	Non-contact localized probing of ferroelectric phase transitions in Li+/Er3+:BaTiO3 ceramics using fluorescence abnormalities. Applied Physics Letters, 2020, 116, .	1.5	5
526	Enhanced mechanical properties in ceramic multilayer composites through integrating crystallographic texture and second-phase toughening. Ceramics International, 2021, 47, 31222-31228.	2.3	5
527	Complete determination of electrostriction tensor components of KMnF3 single crystals at room temperature. Journal of Materials Science Letters, 1988, 7, 327-330.	0.5	4
528	Effects of face plates and edge strips on hydrostatic piezoelectric response of 1-3 composites. Ferroelectrics, 1995, 173, 243-256.	0.3	4
529	Determination of domain and domain wall formation at ferroic transitions. Ferroelectrics, 1999, 222, 1-10.	0.3	4
530	Source excitation methods for the finite-difference time-domain modeling of circuits and devices. Microwave and Optical Technology Letters, 1999, 21, 93-100.	0.9	4
531	Theoretical studies on the pyroelectric properties of two component composite ferroelectric thin film. Physics Letters, Section A: General, Atomic and Solid State Physics, 2006, 360, 357-361.	0.9	4
532	Polarization properties of ferroelectric thin films on transverse ising model. Physica Status Solidi (B): Basic Research, 2008, 245, 2599-2604.	0.7	4
533	Z-scan measurement for the nonlinear absorption of Bi2.55La0.45TiNbO9 thin films. Materials Letters, 2010, 64, 589-591.	1.3	4
534	Effect of lanthanum doping on linear and nonlinear-optical properties of Bi3TiNbO9 thin films. Journal of Alloys and Compounds, 2011, 509, 5364-5367.	2.8	4
535	Biocide silver nanoparticles in two different silica-based coating. AIP Conference Proceedings, 2012, , .	0.3	4
536	Dielectric and elastic properties of 0.70Pb(Mg1/3Nb2/3)O3–0.30PbTiO3 single crystal and their electric-field dependence. Journal of Materials Science, 2012, 47, 429-432.	1.7	4
537	Propagation of Shear Horizontal Waves in Laminated Composites Based on Differently Orientated Poled 0.72Pb(Mg <sub>1/3</sub> Nb <sub>2/3</sub> )O <sub>3</sub> -0.28PbTiO <sub>3</sub> Single Crystals. Chinese Physics Letters, 2013, 30, 096301.	1.3	4
538	Guided Wave Propagation in a Gold Electrode Film on a Pb(Mg 1/3 Nb 2/3 )O 3 â^'33%PbTiO 3 Ferroelectric Single Crystal Substrate. Chinese Physics Letters, 2014, 31, 104302.	1.3	4
539	Diffuse reflectance measurement using gas absorption spectroscopy. Sensors and Actuators B: Chemical, 2014, 196, 147-150.	4.0	4
540	Origin of the deviation between the fluorescence intensity ratio of a thermally coupled level and the Boltzmann distribution law. Europhysics Letters, 2016, 116, 60008.	0.7	4

#	Article	IF	CITATIONS
541	Temperature dependence of full set tensor properties of KTiOPO4 single crystal measured from one sample. Journal of Applied Physics, 2016, 119, 124104.	1.1	4
542	Photoluminescence critical behavior in Er3+ doped Ba0.77Ca0.23TiO3 ceramic. Journal of Alloys and Compounds, 2017, 701, 63-66.	2.8	4
543	Temperature dependence of full matrix material constants of [001]c poled 0.71Pb(Mg1/3Nb2/3)O3-0.29PbTiO3 single crystal. Journal of Applied Physics, 2018, 123, .	1.1	4
544	Accurate characterization of complete set constants of single domain 0.72Pb(Mg1/3Nb2/3)O3–0.28PbTiO3single crystal by resonant ultrasound spectroscopy using only one sample. Journal of Applied Physics, 2019, 125, 064102.	1.1	4
545	Phase stability and Landau phenomenological model of relaxor ferroelectric single crystals 0.78Pb(Mg1/3Nb2/3)O3-0.22PbTiO3. Ceramics International, 2021, 47, 9842-9848.	2.3	4
546	A versatile cryostat and a mutual inductance coil for a.c. susceptibility measurements on high Tc superconductors. Materials Science and Engineering, 1988, 100, L11-L13.	0.1	3
547	Elastic and electric constraints in the formation of ferroelectric domains. Ferroelectrics, 1995, 172, 31-37.	0.3	3
548	Ceramic-metal composite transducers for underwater acoustic applications. , 0, , .		3
549	Effect of defect induced nucleation and growth on switching behavior in ferroelectrics. Ferroelectrics, 2001, 251, 191-198.	0.3	3
550	Efficient determination of resonance frequencies in resonant structures using the FDTD method. Microwave and Optical Technology Letters, 2001, 28, 244-247.	0.9	3
551	Investigation on optical properties of Bi2.85La0.15TiNbO9 thin films by prism coupling technique. Applied Physics A: Materials Science and Processing, 2009, 97, 741-744.	1.1	3
552	Orientation dependence of electromechanical properties of relaxor based ferroelectric single crystals. Journal of Materials Science, 2011, 46, 63-68.	1.7	3
553	Design optimization and experimental study of acoustic transducer in Near Field Acoustic Levitation. , 2011, , .		3
554	Pure low-frequency flexural mode of [011]c poled relaxor-PbTiO3 single crystals excited by k32 mode. Applied Physics Letters, 2012, 100, 213501.	1.5	3
555	Reply to "Comment on â€ <sup>~</sup> Origin of piezoelectric response under a biased scanning probe microscopy tip across a 180° ferroelectric domain wall'― Physical Review B, 2014, 89, .	1.1	3
556	Interactions of collinear acoustic waves propagating along pure mode directions of crystals. Journal of Applied Physics, 2014, 115, .	1.1	3
557	Electromechanical properties of orthorhombic 0.24Pb(In1/2Nb1/2)O3–0.43Pb(Mg1/3Nb2/3)O3–0.33PbTiO3 single-domain crystal. Materials Letters, 2015, 157, 163-165.	1.3	3
558	Effect of high bismuth deficiency on structure and oxide ion conductivity of a Bi <sub>0.55</sub> MoO <sub>4</sub> single crystal. CrystEngComm, 2015, 17, 8746-8751.	1.3	3

#	Article	IF	CITATIONS
559	Determination of full matrix material constants of [111]c poled Mn doped 0.24Pb(In1/2Nb1/2)O3-0.46Pb (Mg1/3Nb2/3)O3-0.30PbTiO3 single-domain single crystal using one sample. Journal of Applied Physics, 2016, 120, .	1.1	3
560	Temperature―and <i>E</i> â€fieldâ€dependent domain configuration and electrical properties in (K, Na,) Tj ETQo 3973-3981.	q0 0 0 rgB 1.9	T /Overlock 3
561	Effect of shear stress in ferroelectric solid solutions with coexisting phases. Journal of Applied Physics, 2017, 122, .	1.1	3
562	Low-frequency Gibbs-type oscillation in finite solid–fluid sonic crystals and its application in sub-wavelength wave isolation for waterborne sound. Journal Physics D: Applied Physics, 2019, 52, 505114.	1.3	3
563	Temperature Dependence of Normalized Sensitivity of Love Wave Sensor of Unidirectional Carbon Fiber Epoxy Composite on Mn-Doped 0.24PIN-0.46PMN-0.30PT Single Crystal Substrate. Applied Sciences (Switzerland), 2020, 10, 8442.	1.3	3
564	Simulation of the Dynamical Behavior of 1-3 Piezocomposite Using Finite Element Method. Ceramic Engineering and Science Proceedings, 0, , 83-90.	0.1	3
565	Temperature dependence of electrical and optical properties in Eu3+ doped Pb(Mg1/3Nb2/3)O3-PbZrO3-PbTiO3 ferroelectric ceramics. Journal of Alloys and Compounds, 2022, 897, 163162.	2.8	3
566	Temperature- and electric field-dependence of polarization hysteresis for a [001] <sub>c</sub> poled PMN-PT single crystal. Journal of Asian Ceramic Societies, 2022, 10, 203-214.	1.0	3
567	<title>Finite element study on random design of 2-2 composite transducer</title> . , 1997, , .		2
568	<title>Finite element and experimental study of composite and 1D array transducers</title> ., 1998, , .		2
569	Observation of ferroelectric domains in LiTaO3. Ferroelectrics, 1999, 226, 27-35.	0.3	2
570	FDTD study of resonance processes in microstrip ring resonators with different excitation geometries. , 0, , .		2
571	Numerical modeling and experimental investigation of resonance properties of microwave capacitors. Microwave and Optical Technology Letters, 2001, 29, 54-60.	0.9	2
572	Orientational twins in an improper ferroelastic phase transition driven by theM5â^'zone-boundary phonon inRAg1â^'xInx. Physical Review B, 2002, 65, .	1.1	2
573	FDTD study of surface waves in microstrip and patch structures. , 0, , .		2
574	Observation of Ferroelectric Domains using Environmental SEM. Microscopy and Microanalysis, 2004, 10, 1072-1073.	0.2	2
575	Study of electric-field-induced phase transitions in [111] oriented 0.955Pb(Zn1/3Nb2/3)O3–0.045PbTiO3 single crystals. Materials Letters, 2005, 59, 3276-3279.	1.3	2
576	Nano-structured TiO <sub>2</sub> film fabricated at room temperature and its acoustic properties. Journal Physics D: Applied Physics, 2008, 41, 162001.	1.3	2

#	Article	IF	CITATIONS
577	Polarization fatigue and photoinduced current in (Pb0.72La0.28)Ti0.93O3 buffered Pb(Zr0.52Ti0.48)O3 films on platinized silicon. Materials Research Bulletin, 2009, 44, 803-806.	2.7	2
578	Orientation dependence of coupling between Lamb and shear horizontal waves in (1-x)Pb(Mg <inf>1/3</inf> Nb <inf>2/3</inf> )O <inf>3</inf> -xPbTiO <inf>3</inf> single crystal plates. , 2009, , .		2
579	High sensitivity gravimetric sensor made of unidirectional carbon fiber epoxy composite on (1 â^' x) Tj ETQq1 I	. 0.784314 0.7	rgBT /Overloo
580	Effects of surroundings on upconversion luminescent properties of rare earth luminescence centers. CrystEngComm, 2014, 16, 9974-9978.	1.3	2
581	Influence of poling condition on crystal-rod domain configuration in 0.67Pb(Mg 1/3 Nb 2/3 )O 3 -0.33PbTiO 3 single crystal/epoxy 1-3 composites. Journal of Alloys and Compounds, 2017, 699, 442-447.	2.8	2
582	Precise determination on the upconversion processes of the ultraviolet upconversion fluorescence of Ho^3+-doped Y_2O_3 ceramic by excitation of a 532-nm continuous-wave laser. Optics Letters, 2017, 42, 2279.	1.7	2
583	Differentiate low impedance media in closed steel tank using ultrasonic wave tunneling. Ultrasonics, 2018, 82, 130-133.	2.1	2
584	Enhanced electrocaloric effect in a Si-doped PbZr0.95Ti0.05O3 film deposited on FTO substrate. Applied Physics Letters, 2019, 115, 053901.	1.5	2
585	Ferroelectric properties of Ag doped PbZr0.53Ti0.47O3 thin film deposited by sol–gel process. Journal of Materials Science: Materials in Electronics, 2019, 30, 2592-2599.	1.1	2
586	Phase field simulation of de-aging process in acceptor-doped ferroelectrics. Journal of Alloys and Compounds, 2020, 816, 152503.	2.8	2
587	Temperature- and electric-field-dependent electrical properties and nanoscale domain structures in PIN-0.49PMN-0.27ÂPT single crystal. Ceramics International, 2021, 47, 25875-25882.	2.3	2
588	Multifunctional Materials $\hat{a} {\in} "$ the Basis for Adaptronics. , 1999, , 35-57.		2
589	Phase-field simulation on the interaction of oxygen vacancies with charged and neutral domain walls in hexagonal YMnO <sub>3</sub> . Journal of Physics Condensed Matter, 2022, 34, 165401.	0.7	2
590	Preparation variables for the GdBa2Cu3O6.5+l̂´ superconductive ceramics. Materials Research Bulletin, 1988, 23, 421-428.	2.7	1
591	Optical absorption from polarons and bipolarons in a tetrahedrally bonded homopolymer. Physical Review B, 1988, 38, 1800-1805.	1.1	1
592	The twin structures and the piezoelectric effect in ferroelectric ceramics. Ferroelectrics, 1991, 120, 55-56.	0.3	1
593	Electric fatigue initiated by surface contamination in high polarization ceramics. , 0, , .		1
594	Strain profile and piezoelectric performance of piezocomposites with 2-2 and 1-3 connectivities. , 0, , .		1

#	Article	IF	CITATIONS
595	<title>Finite element and experimental study of impedance matching layer optimization</title> . , 1997, , .		1
596	<title>Transducer design simulation using finite element method</title> ., 1997,,.		1
597	<title>Virtual design of medical transducers</title> ., 1998, , .		1
598	Elastic property characterization in thin samples of sub-wavelength in thickness. Ferroelectrics, 1998, 206, 355-363.	0.3	1
599	A guided acoustic wave method for characterization of medical ultrasound transducers. , 0, , .		1
600	Imaging of ferroelectric domains in LiTaO3by enviromental scanning electron microscopy. Ferroelectrics, 1999, 222, 257-262.	0.3	1
601	Finite-difference time-domain simulation of resonant modes of rectangular dielectric resonators. Microwave and Optical Technology Letters, 2003, 36, 160-164.	0.9	1
602	Finite element study of 2-2 piezocomposite transducer with random polymer properties. , 2003, , .		1
603	Time evolution of polar regions in (Sr0.65Ba0.35)2NaNb5O15single crystal. Phase Transitions, 2006, 79, 513-524.	0.6	1
604	Multifunctional Materials: The Basis for Adaptronics. , 2007, , 29-53.		1
605	Electric field dependence of nonlinearity parameters and third order elastic constants of 0.70Pb(Mg1/3Nb2/3)O3–0.30PbTiO3 single crystal. Applied Physics Letters, 2010, 96, 052905.	1.5	1
606	High Concentration Silver/Organic or Silver/Inorganic Nanocomposites and Their Optical Properties. , 2011, , .		1
607	Poling induced higher order nonlinearity changes in lead zirconate titanate ceramic. Solid State Communications, 2012, 152, 165-167.	0.9	1
608	New method for measuring time-resolved spectra of lanthanide emission using square-wave excitation. Review of Scientific Instruments, 2013, 84, 113106.	0.6	1
609	<i>k</i> <sub>32</sub> â€type lowâ€frequency bimorph with giant electromechanical coupling factor. Physica Status Solidi (A) Applications and Materials Science, 2013, 210, 2183-2187.	0.8	1
610	Eliminating the "decoupling―effect of fluorescence intensity ratio thermometry for an upconversion pumped system. Journal of Luminescence, 2017, 192, 184-187.	1.5	1
611	Effects of polymeric filler on polarization fatigue of 1-3 0.74Pb(Mg1/3Nb2/3)O3-0.26PbTiO3 single crystal/polymer composites. Journal of Applied Physics, 2018, 124, .	1.1	1
612	Aging and thermal stability of [001]c- and [111]c-poled 0.63Pb(Mg1/3Nb2/3)O3–0.37PbTiO3 single crystals. Journal of Materials Science: Materials in Electronics, 2018, 29, 16207-16214.	1.1	1

#	Article	IF	CITATIONS
613	Elimination of Severe Near-Field Spatial Variations of Ultrasonic Transducers Using γ-Power Bessel Function Amplitude Distribution. Physical Review Applied, 2019, 12, .	1.5	1
614	NIR Photocatalysis: Plasmonic Enhanced Reactive Oxygen Species Activation on Lowâ€Workâ€Function Tungsten Nitride for Direct Nearâ€Infrared Driven Photocatalysis (Small 45/2020). Small, 2020, 16, 2070247.	5.2	1
615	Energy Integration Method for Calculating <i>k</i> <sub>eff</sub> and its Application in Design Optimization of Disk Resonators via Convex Edge. IEEE Transactions on Ultrasonics, Ferroelectrics, and Frequency Control, 2021, 68, 734-741.	1.7	1
616	Second harmonic generation of shear waves in crystals. IEEE Transactions on Ultrasonics, Ferroelectrics, and Frequency Control, 2004, 51, 153-62.	1.7	1
617	Characterizing ultra-thin matching layers of high-frequency ultrasonic transducer based on impedance matching principle. IEEE Transactions on Ultrasonics, Ferroelectrics, and Frequency Control, 2004, 51, 211-5.	1.7	1
618	Computer-aided characterization of ferroelectric phase transitions and domain structures using polarizing light microscopy. Applied Physics Letters, 2022, 120, 072902.	1.5	1
619	Dependence of coercive field of PIN–PMN–PT single crystal on temperature and frequency. Journal of Applied Physics, 2022, 131, 124102.	1.1	1
620	Title is missing!. Journal of Materials Science Letters, 2001, 20, 2105-2107.	0.5	0
621	P3K-2 Fabrication and Characterization of Nanocrystalline TiO2-Polymer Composite Matching Layers. Proceedings IEEE Ultrasonics Symposium, 2007, , .	0.0	0
622	Phase transformation properties of finite size ferroelectric thin film with structural transition zones. Journal of Applied Physics, 2008, 104, .	1.1	0
623	Pyroelectric properties of finite size ferroelectric thin films with structural transition zones. Physica B: Condensed Matter, 2009, 404, 2028-2033.	1.3	0
624	Pyroelectric Study on Dipolar Alignment in 0.69Pb(Mg <sub>1/3</sub> Nb <sub>2/3</sub> )O <sub>3</sub> -0.31PbTiO <sub>3</sub> Single Crystals. Chinese Physics Letters, 2012, 29, 047702.	1.3	0
625	<i>In vivo</i> integrated photoacoustic ophthalmoscopy, optical coherence tomography, and scanning laser ophthalmoscopy for retinal imaging. , 2012, , .		0
626	Elastic anomalies near phase transitions of lead-free (Na,Bi)TiO3 and (Ba,Zr)TiO3 ferroelectric ceramics. Science Bulletin, 2014, 59, 2287-2291.	1.7	0
627	Polarized Raman study on phase transitions of the nanodomains in 0.24Pb(In1/2Nb1/2)O3–0.43Pb(Mg1/3Nb2/3)O3–0.33PbTiO3ferroelectric single crystal. Integrated Ferroelectrics, 2016, 170, 155-161.	0.3	0
628	Er <sup>3+</sup> doped Pb(Mg <sub>1/3</sub> Nb <sub>2/3</sub> )O <sub>3</sub> -0.25PbTiO <sub>3</sub> transparent ceramic: a multi-functional material for photonics switching and temperature measurement. Proceedings of SPIE, 2017, , .	0.8	0
629	Ultrasonic pulse-echo technique for the characterization of elastic constants of single domain Pb(Zn1/3Nb2/3)O3–5.5%PbTiO3 single crystals with 3m symmetry. Journal of Materials Science, 2020, 55, 12737-12746.	1.7	0
630	Sinoporphyrin sodium mediated sonodynamic therapy generates superoxide anion under hypoxia environment. New Journal of Chemistry, 0, , .	1.4	0

#	Article	lF	CITATIONS
631	The Abnormal Physicochemical Phenomena of Singlet Oxygen Sensor Green in Water in the Presence of Ultrasound. ChemistrySelect, 2021, 6, 6631-6635.	0.7	0
632	Involvement of hydrogen peroxide in sonodynamical effect with sinoporphyrin sodium in hypoxic situation. Free Radical Research, 2021, 55, 958-969.	1.5	0
633	Heterogeneous Nucleation in a 2-D Model of Martensitic Transformation with Volume Changes. Solid Mechanics and Its Applications, 2002, , 213-220.	0.1	0
634	The need of electron microscopy in the study of domains and domain walls in ferroelectrics. Proceedings Annual Meeting Electron Microscopy Society of America, 1994, 52, 550-551.	0.0	0
635	Design simulation of composite transducers. Journal of the Acoustical Society of America, 1997, 101, 3141-3141.	0.5	0
636	Application of fluorescence spectroscopy and imaging in the detection of a photosensitizer in photodynamic therapy. , 2017, , .		0
637	Temperature and frequency dependent defect dipole kinematics in "hard" piezoelectric ceramics. Sensors and Actuators A: Physical, 2022, 344, 113712.	2.0	Ο